Study of the partitioning of the water vapour flux exchanged by ecosystems between transpiration and evaporation

Auteur : Cravatte, Clara
Promoteur(s) : Heinesch, Bernard; Rothfuss, Youri
Faculté : Gembloux Agro-Bio Tech (GxABT)
Diplôme : Master en bioingénieur : sciences et technologies de l'environnement, à finalité spécialisée
Année académique : 2020-2021
URI/URL : http://hdl.handle.net/2268.2/12889

LIÈGE université
Gembloux
Agro-Bio Tech

STUDY OF THE PARTITIONING OF THE WATER VAPOUR FLUX EXCHANGED BY ECOSYSTEMS BETWEEN TRANSPIRATION AND EVAPORATION

CLARA CRAVATTE

MASTER THESIS PRESENTED IN VIEW OF OBTAINING THE DIPLOMA OF

MASTER BIOENGINEER IN ENVIRONMENTAL SCIENCES AND TECHNOLOGIES.

ACADEMIC YEAR 2020-2021

CO-PROMOTERS: HEINESCH BERNARD – ROTHFUSS YOURI

[1] In this case, the academic authority is represented by the promoter(s) member(s) of the GxABT teaching personnel.

LIÈGE université
Gembloux
Agro-Bio Tech

STUDY OF THE PARTITIONING OF THE WATER VAPOUR FLUX EXCHANGED BY ECOSYSTEMS BETWEEN TRANSPIRATION AND EVAPORATION

CLARA CRAVATTE

MASTER THESIS PRESENTED IN VIEW OF OBTAINING THE DIPLOMA OF

MASTER BIOENGINEER IN ENVIRONMENTAL SCIENCES AND TECHNOLOGIES.

ACADEMIC YEAR 2020-2021

CO-PROMOTERS: HEINESCH BERNARD – ROTHFUSS YOURI

Acknowledgments

In the framework of this research Master Thesis, I have been lucky enough to work with some great people I would like to thank here.

First of all, I would like to thank my promoters, Bernard Heinesch and Youri Rothfuss, who have guided and advised me throughout this work. Their investment and support have been a great help in the realisation of this project of which I am very proud.

Secondly, I would like to warmly thank Ariane Faurès for the access to the data that was necessary for my work, but also for her availability and the constructive discussions that fed my reflections.

I would also like to thank Quentin Beauclaire for our discussions, which were of great help to me.

A great thanks to Anne Klosterhalfen, Todd Skaggs, and Alexander Graff for helping me and giving insight when I was struggling with the application of Fluxpart.

A special thanks to my jury's members who agreed to be involved in the evaluation of the present work.

Finally, I would like to thank Gembloux Agro-bio Tech for these wonderful years of rich learning, during which I had the opportunity to grow and gain maturity in an environment that was always caring.

Thank you to my family, my friends and Maxime.

Abstract

Climate change is expected to dramatically impact our activities, especially agriculture. Farmers have to face the challenge of feeding an ever-growing population with increasingly limited resources, notably water resources. Improving water management strategies and policies is therefore key to tackling this challenge. To this end, the study of the evapotranspiration (ET) partitioning into its main components is needed to identify the productive fraction of this flux (i.e., transpiration) and to limit evaporation (E). In this work, a recent partitioning model was used, Fluxpart. A sensitivity analysis to its main parameters was conducted, its partitioning performances were assessed, and the model was compared to another well-established and validated partitioning model, AquaCrop. In addition to this, the impact of considering transpiration (T) instead of ET in determining the canopy resistance via the application of the Penman-Monteith equation was investigated. Indeed, the assumption of equality between T and ET is often made but can lead to errors. These were quantified in the present work. The main outcomes of this study were that Fluxpart failed to partition a significant number of half-hours. The fact that the partition succeeded or not seemed to be linked to the stability parameter, but further research is needed to confirm this intuition. Concerning the performances of Fluxpart, although the general dynamics of the partitioning computed by the two models are identical and consistent with the literature, significant differences in the importance of the partitioned fluxes were observed between the Fluxpart's partition and the AquaCrop's partition. One should note that the number of half-hours, for which the partition failed was too important to implement Fluxpart routinely with an eddy-covariance station measurement. Further research should then be conducted on Fluxpart, its partitioning success and its possible link to the stability parameter. Other recent models should also be investigated, such as the model developed by Li and colleagues, which also looks very promising, according to the literature.

Résumé

Le changement climatique va modifier drastiquement nos activités, notamment l'agriculture. Les agriculteurs doivent déjà faire face au défi de nourrir une population toujours grandissante avec des ressources toujours plus limitées, notamment en eau. L'amélioration de la gestion de cette ressource est donc essentielle pour réussir ce défi. A cette fin, il est nécessaire d'étudier la partition de l'évapotranspiration en ses composantes principales pour identifier la fraction productive de ce flux (c'est-à-dire la transpiration) et pour limiter l'évaporation. Dans le présent travail, Fluxpart, un récent modèle de partition, est utilisée. Une analyse de sensibilité aux paramètres principaux du modèle est réalisée, les performances de ce modèle sont évaluées et il est comparé à un autre modèle, lui bien établi et validé, AquaCrop. En plus de cela, l'impact du fait de considérer la transpiration à la place de l'évapotranspiration dans le calcul de la résistance de canopée via l'application de l'équation de Penman-Monteith est étudié. En effet, l'hypothèse d'égalité entre les flux de transpiration et d'évapotranspiration est souvent faite, mais peut mener à d'importantes erreurs. Ces dernières sont quantifiées dans le présent travail. Les résultats principaux de cette étude montrent que Fluxpart échoue à partitionner un nombre significatif de demi-heures. Le fait que la partition réussisse ou ne réussisse pas semble lié à la stabilité atmosphérique, mais de plus amples recherches sont nécessaires pour confirmer cette intuition. En ce qui concerne les performances de Fluxpart, bien que les dynamiques générales de la partition soient identiques pour les deux modèles et concordent avec la littérature, des différences significatives ont été observées entre l'importance des flux simulés par Fluxpart et par AquaCrop. Il est bon de noter que le nombre trop important de demi-heures pour lesquelles la partition a échoué est trop élevé que pour pouvoir implémenter Fluxpart en routine dans une station de mesure par eddy-covariance. De plus amples recherches devraient être menées sur Fluxpart, le succès de sa partition et son possible lien avec la stabilité atmosphérique. D'autres modèles récents devraient également être plus étudiés, comme le modèle développé par Li et ses collègues, qui a également l'air prometteur d'après la littérature.

Figure list

Table list

TABLE OF CONTENTS

1 Introduction

1.1 Rationale

Evapotranspiration (ET) is a water flux including soil evaporation (E) from the soil surface, interception from the canopy and plant transpiration (T) [1].The E flux from the soil surface is a complex process involving soil characteristics and evaporative atmospheric demand [2]. Interception from the canopy represents the water quantity intercepted by the vegetation during a rainfall event that will return to the atmosphere via an evaporative phenomenon [3]. These two fluxes therefore depend only on abiotic processes. In contrast, T is governed also by biotic processes. Indeed, the latter represents the flux of water moving across the soil-plant-atmosphere continuum [4]. It should be noted that these fluxes are interdependent, i.e., under certain conditions, E from the soil can form a micro-climate that allows a T regulation [5].

The study of ET is key to better understand climate change [5]. Notably through its linkage with the carbon cycle [6]. Despite this fact, it is still unclear whether ET flux increases or decreases, causing an acceleration or a deceleration of the water cycle at a global scale [7]. A better understanding of ET is then crucial to better predict future climate [1]. One prerequisite for this is the partitioning of ET into its main components [5].

Although T and E are important in terms of water and energy balance of soils, they do not have both the same usefulness regarding the manner we use the soils [3]. Indeed, T is the only flux beneficial to the vegetation's development [8]. In contrast, E is seen as an undesirable part of ET as the precipitated water returns directly to the atmosphere without having benefited the vegetation [5].

As a significant part of the earth already suffers from limited water supply and this trend will only intensify in the future, it is imperative to limit any form of water waste [9]. This means reducing as much as possible the fraction of ET imputable to E in agricultural ecosystems by using appropriate management practices [5]. Water resources management is all the more important as the world population will continue to grow in the next decades [10]. The main challenge for the farmer of tomorrow will be to feed more people using less freshwater. This can be achieved by choosing the agricultural practices that reduces the most the E fraction. This demonstrates the urgent need to develop, calibrate and validate models capable of partitioning ET into its main components [5].

This partitioning is also important in other fields such as the study of contaminants movements in soils. Indeed, if E is the dominant flux component in ET, contaminants concentrate more at the soil surface, whereas a dominant T flux would causes a contaminant accumulation in the root zone [11].

ET partitioning is also relevant for the determination of pivotal physiological parameters such as canopy resistance requires knowledge of T. Generally, the assumption saying that ET is equal to T is made. This can be acceptable for fully developed canopy covers but, in sparsely vegetated areas, E can represent a non-negligeable fraction of ET [5]. This approximation may lead to a significant bias in the computed parameters. This partition is thus important to link physiological features such as canopy resistance, biomass production, agricultural yield, among others, and the water cycle through the ET components.

1.2 State of art

The interest in partitioning ET is not new. A range of partitioning methods already exists to compute this partition [5], [7]. The present section is strongly inspired by the previous reviews written by Kools and al., (2014) and Stoy and al., (2019). More information can be found about the following models in these reviews. Here, only a brief overview of the panel of possible techniques is presented. Typically, the models are categorized into empirical and mechanistic approaches. More categories are described here to be as relatable as possible to the philosophy of the presented models.

The first model is the FAO dual-Kc. In this empirical approach, a crop-specific multiplication factor combined to a reference ET is defined to computes aboveground biomass for a well-watered crop [12]. To partition ET, the dual-Kc approach separates this factor into a plant component and a soil component. E and T are then calculated based on these factors. This method is one of the most commonly used because its finesse can be adapted regarding the available measures and requires classical measures. In addition to this, the results are accurate enough to be used in an agricultural framework [5]. A second empirical approach uses the natural properties of water stable isotopes. The hydrogen and oxygen atoms composing the water molecule have stable isotopes, which differ in their mass.[13] As the ratio of concentration between heavier and lighter hydrogen and oxygen isotopes is greater in the more condensed phase (i.e. liquid water as compared to the atmospheric water vapor and evaporative flux) because of the so-called fractionation process, it can be used to trace the movement of water through hydrologic pathways [7], [14]. The difference in the water isotopic concentration ratio of the E, T, and ET fluxes (R_E, R_T, and R_{ET}) forms the basis for the isotopic partitioning of ET [13]. A simple mass balance leads to the following equation:

$$\frac{T}{ET} = \frac{R_{ET} - R_E}{R_T - R_E} \tag{1.2.1}$$

Despite its successful application in many studies [15], this method is not widely used in the agronomic field yet because of its cost, complexity and low time resolution [5].

The mechanistic category includes several models such as the Shuttleworth-Wallace model, HYDRUS-1D, the energy and water balance (ENWATBAL) model, Cupid-DPEVAP and the soil, water, energy, and transpiration (SWEAT) model. The Shuttleworth-Wallace model is an analytical model based on two Penman-Monteith equations [16], [17]. One equation relates to the crop T while the other to soil surface E [18]. Even if this model is rarely used in practical because of the complexity of its parametrisation, it is the basis of many more recent ET partitioning models [5]. The Cupid-DPEVAP model stems from the combination of the plant-environment energy balance (Cupid) model and the water droplet evaporation-trajectory (DPEVAP) model [5]. Its aim is to partition ET under sprinkler irrigation. The principle of this model is to create classes of leaf angles and solve a leaf energy balance for each of these classes. Cupid-DPEVAP showed good agreement with sap-flow measurement, but it generally seems to slightly overestimate E [5]. The next three models are still in the mechanistic category but are, this time, numerical ones. ENWATBAL is a model developed to compute the water and energy balances both at soil surface and at the canopy surface [5]. This model requires information about soil, plants, and atmospheric inputs. Its performances were tested in diverse studies and the results showed good agreement with observations [19]. Concerning the SWEAT model, the ET partitioning computation is based on a two-layer approach (soil and canopy). The originality of this approach lies in the fact that the calculation doesn't require a soil resistance parameter but requires leaf area index, vegetation height measurement and meteorological data [20]. The last model presented in this category is HYDRUS-1D. This model simulates water, heat, and solute movements via the solving of Richards' equation and Fick's law [5]. In HYDRUS-1D, E is constrained by both the atmospheric demand and the soil hydraulic conductivity while T is constrained by the rate at which

water can be transported in the root zone [5]. However, this model was compared to the isotopic partitioning approach and the differences in the partitioning computed with this approach were significant, which suggests that the HYDRUS-1D method needs further validation [21]–[23].

Another modelling category uses remote sensing data and includes three different models. The first one is the extended remote sensing method, which can be used not only to determine ET, but also for the purpose of partitioning. ET can be determined by applying an ecosystem energy balance residual approach [7], [24]. In addition, E and T can be quantified from the surface, from which they arise from radiometric surface temperature observations at fine spatial and temporal resolutions [7], [25]. This method has been applied in several studies all focusing on soil E [26] and plant T [25] independently. This method is now widely used at study sites to measure the temperature of different ecosystem components at high temporal and spatial resolution [7], [27], [28]. The second model included in this approach is the two-source energy balance (TSEB). The needed inputs are [5]: (i) radiometric surface temperature, (ii) meteorological data, and (iii) canopy characteristic. This model is based on two energy balance equations, one applied to the soil and the other applied to the canopy [5]. Studies showed that the TSEB could be applied to a large scale because of the few inputs needed and the possibility of acquiring a subset of them using remote sensing [29]. The last model featured in this category is based on the solar-induced fluorescence (SIF). The SIF is the process by which some of the incoming radiation is absorbed by the leaf and reemitted by chlorophyll [7], [30]–[32] and can be quantified on hand of remote sensing data. This approach is interesting for ET partitioning because SIF emissions are related to photosynthesis, which is linked to T via stomatal conductance and drivers [33], [34], recent studies proposed to used SIF as a T monitor.

Another category is statistically based. The only model being part of this category is the evapotranspiration from relative humidity in equilibrium (ETRHEQ) model. It is based on the hypothesis that the best-fit daily surface conductance minimizes the vertical variance of relative humidity averaged over the day [35]. This method requires the following inputs to be informed at an hourly timestep: (i) temperature, (ii) humidity, (iii) pressure, (iv) wind speed, (v) solar radiation, (vi) vegetation height, (vii) surface emissivity, (viii) thermal soil inertia, and (ix) soil moisture [36]. These inputs allow for disentangling the computed surface conductance into soil and vegetation conductances [7]. The underlying assumption of this theory is that the vegetation and soil respond independently to environmental variations [36]. Even if there is a lack of evaluation of this model with direct observations of E and T, estimates of T showed good agreement with other partitioning methods such as SIF and realistic dry-down period dynamics [7].

The final category described in this work is related to eddy-covariance measurements. Several applications of the eddy-covariance method allow for partitioning ET. The first one is the ET partitioning using half-hourly eddy-covariance observations, in which it may be assumed that ET is solely composed by E in the absence of gross primary production (GPP) because of the coupling between carbon dioxide and water vapour fluxes through plant stomata [7], [37]. In addition to this, it is assumed that E can be estimated by simulating solar radiation attenuation through the canopy. T is then estimated as the difference between measured ET and simulated E when GPP occurs [7]. Note that this method could not be validated because of the lack of E measurements. Another example of ET partitioning using half-hourly eddy-covariance observations is the concurrent above- and below-canopy eddy-covariance measurements in forest ecosystems [7], [38]. However, this method was mostly applied to carbon dioxide flux partitioning so far [7], [39]. A last example of partitioning method based on half-hourly eddy-covariance observations that will be covered in this work is based on the optimality theory assumption that plants minimize water loss per unit of CO_2 gain [40]. The results obtained from studies in forest ecosystems showed good agreement of the T/ET temporal dynamics

with the isotopic approach [41]. Other authors developed methods relying on the same theory. An example of this is the use of a big-leaf canopy model in which parameters were optimized based on a half-hourly data in 5-days windows [42]. One last method worth mentioning is the transpiration estimation algorithm (TEA).[43] The advantage of this non-parametric approach is that this limits the assumptions made about ecosystem functions [7]. Another application of the eddy-covariance principle is the study of the carbonyl sulfide fluxes (COS). Carbonyl sulfide is a trace gas present in the atmosphere at an average concentration of 500 ppt [7], [44]; it can be used to estimate GPP and the canopy conductance (and thus T with water vapour concentration measurements) because plants draw CO_2 and COS at the same time from the atmosphere. This means that both gas have common boundary layer and stomatal conductance as they follow a similar diffusive pathway [7], [45]–[47]. An additional interesting feature of the use of COS to estimate GPP is that COS leaf exchange is generally unidirectional [45]. Although this method shows potential and can be applied via the measurement of COS concentration by eddy-covariance, precautions are to be taken [48]. Indeed, it is not only vegetation that interacts with COS, but soils can also release and take up COS, especially in agricultural ecosystems [49]. Ecosystem-scale COS flux measurements need to account for any soil exchange, although the soil contribution is typically small [7], [50], [51]. The last application of eddy-covariance measurements that will be presented in this work is the correlation-based ET partitioning approach. This partitioning method developed by Scanlon and Kustas (2010) and Scanlon and Sahu (2008) is based on high-frequency eddy-covariance measurements and the Monin-Obukhov similarity theory [7], [54]. As this approach is used in the present work, it will be detailed in section 2.3.

Even if all these models and approaches seem promising, they often rely on assumptions that need to be further tested. Additional studies dedicated to assess, evaluate and compare these models should then be carried out with the aim of developing the most accurate ET partitioning model [5], [7]. Independent measurement techniques of E and T are not described in the present work for the sake of conciseness. However, it is important to mention that no independent measurements were available to validate the partitioning computed in the framework of this study. This is because the measurement methods were either at too fine spatial scale, which would lead to all the upscaling difficulties, or because the installation was too complex to be implemented for this project.

1.3 Definition of the Master Thesis objectives

In the present work, E and T fluxes were sought at a spatial scale of a parcel and a half-hourly time scale. ET measurements were available at these spatial and time scales as well as other typical flux tower measurements. Possible ET partitioning methods were investigated based on these available measurements. The correlation-based method was selected and more precisely, the Flux-Variance Similarity theory (FVS). This method was chosen for several reasons. The first one is because it requires high frequency raw eddy-covariance data that is ordinarily collected on flux tower sites. The second reason is that it is a direct method, even if it relies on assumptions that will be developed in greater detail latter, that could be applied to historical datasets. The next reason is that it is publicly accessible as a software. The final reason why this method was chosen is because it is a recently developed method that needs to be tested. In the absence of measurement to validate the partitioning, FAO dual-Kc was also applied. This second method was chosen also because of its wide validation across crops and climates. In addition to this, these models are conceptually very different and so are their aims. FVS is a recent approach developed to study in detail carbon dioxide and water vapour fluxes while FAO dual-Kc was developed to predict biomass production or to provide irrigation schedules based on meteorological, soil and crop data. FAO dual-Kc is intended to be used by people with basic prior theoretical knowledge on ET partitioning while FVS is first intended for the research community. In addition to this, the influence of considering T instead of ET in the determination of the canopy resistance using the Penman-Monteith equation was also studied in this work. Note that only T and E were considered in the present work as the interception is negligible in non-forest canopies [5].

The objectives of this work are therefore the following: (i) partition ET into E and T using the FVS and FAO dual-Kc methods, (ii) compare the two methods and estimate their robustness through the characterization of E and T temporal dynamics, and (iii) evaluate the impact of the partitioning on the canopy resistance estimation.

2 Material and methods

2.1 Study site and data treatment

2.1.1 Study site

The study site is located in Lonzee, Belgium (50°33'5.8''N – 4°44'46.5''E). It has been instrumented first in 2004 and is part of the ICOS[2] ecosystem flux station network since 2018. The average altitude is 170m above sea level and the climate is temperate oceanic. The main wind direction is South-West, the annual precipitation is approximatively 800 mm and the mean annual temperature is approximatively 10°C [55].

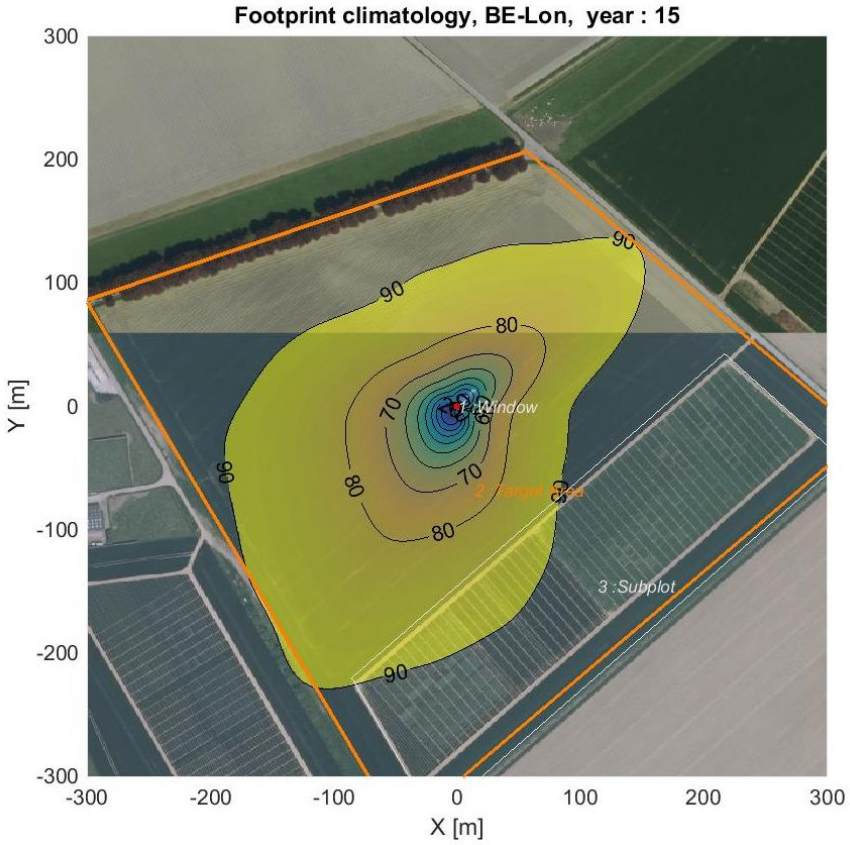

Figure 1 - Aerial view of the site (the target area is the orange polygon) and representation of the flux footprint.

The area of interest (Figure 1) is a 12-ha field that has been cultivated for the last 75 years. A 4-year basis rotation (sugar beet, winter wheat, potato, winter wheat) was initiated in 2000. During the 2014-2015 growing season, winter wheat (*Triticum aestivum* L. cv. Sahara) was cultivated. This crop was sowed on the 14th of October 2014 (DoY 287) and harvested on the 2nd of Augustus 2015 (DoY 214). Nitrogen fertilizer has been applied 3 times during this period (DoY 73, 105 and 131), a growth regulator, an insecticide, and a fungicide were applied each once on DoY 105, 328, and 146, respectively. The soil's first meter in the area of interest is a silt loam (5.6 – 8.2% sand, 74.7 – 80.2% silt, 11.6 – 19.7% clay) and presents an imperfect to favourable drainage. A shallow water table of variable depth is present at the site. The maximum slope observed in this location is 1.32%.

The field is equipped with an eddy-covariance mast operating at a 20 Hz sampling frequency. It measures wind speed and wind direction using a sonic anemometer (Solent Research HS-50, Gill

[2] Integrated Carbon Observation System, https://www.icos-cp.eu/ and also https://www.icos-belgium.be/ESLonzeeData.php

Instruments Lymington, UK) at a height of 2.8 meters and CO_2 and H_2O mixing ratios using an infrared gas analyser (LI-7200, LI-COR, Lincoln, NE, US), sampling air at a height of 2.8 meters. This set-up was complemented by a meteorological station, of which the details (device types and references, and installation height) can be found in Table 1.

Table 1 – Description of the devices presents on site.

Variable measured	Device	Reference	Installation height [m]
Wind speed Wind direction	Sonic anemometer	Solent Research HS-50, Gill Instruments Lymington, UK	2.8
CO2 and H2O concentration	Infrared gas analyser	LI-7200, LI-COR, Lincoln, NE, US	2.8
Solar radiation Terrestrial radiation	Pyrradiometer	CNR 4, Kipp and Zonen, Delft, NL	2.8
Photosynthetic photon flux density	Photo-receptor cells	PAR Quantum sensor SKP 215 Skye Instruments Limited, Llandrindod Wells, UK	2.88 2.65
Precipitation	Weighing rain gauge	TRwS415, MPS system sro, Bratislava, Slovakia	1.1
Air temperature Air humidity	Thermistor and electrical capacitive hygrometer	RHT2nl, Delta-T Devices Ltd, Cambridge, UK	2.8 1.0 0.3
Atmospheric pressure	Barometer	PTB110/CS106, Campbell Scientific, Logan, UT, US	1.0
Soil temperature	Electrical resistance thermometer	PT 107, Campbell Scientific, Logan, UT, US	-0.01 -0.05 -0.15 -0.25 -0.45
Soil moisture	Time domain reflectometer	CS616, Campbell Scientific, Logan, UT, US	-0.01 -0.05 -0.15 -0.25 -0.45
Soil heat flux	Self-calibrating soil heat flux plate	HFP01SC, Hukseflux Thermal Sensors B.V., Delft, NL	-0.05
Water table depth	Pressure transducer	ED752, Baumer, Frauenfeld, CH	-3
Canopy temperature	Infra-red remote temperature sensor	IR 120, Campbell Scientific, Logan, UT, US	2

Regarding the phenological variables, the green area index (GAI) was measured through destructive sampling following the ICOS prescriptions. The crop height was manually measured using a graduated stick.

2.1.2 Eddy-covariance data processing

The method of acquiring and processing eddy-covariance data is detailed in a reference article [56]. Therefore, only a brief description will be given in this document.

Fluxes of CO_2, water vapour and sensible heat were measured by the eddy-covariance system described in the section 2.1.1. The raw data was processed using EDDYFLUX, from the eddy-covariance software package EDDYSOFT [57]. Fluxes were calculated using the processing options reported below

(Table 2) and well established in the flux community for this type of instrumentation, ecosystem, and topography:

Table 2 – Processing options for fluxes calculation.

Raw data processing	Despiking
Average flux period	30 minutes
Time lag computation	Covariance maximisation with default value
Detrend method	Block average
Coordinate rotation	2D

Because of the system setup (e.g., tube length, sensor separation), the turbulent signal in the high frequency range is not fully measured by the sensors (low-pass filtering). There is therefore a systematic under-estimation of the final fluxes. There are several methods available to account and correct for these high frequency losses. Here, the co-spectral experimental approach was applied [56]. Footprint-based data filtering should ensure selection of half-hours with fluxes originating mainly from the target area, the footprint being "upwind source areas to downwind fluxes " [58]. One might finally note that the high frequency losses correction and the instruments' calibration is of crucial importance, especially for the water vapour fluxes measurements.

2.2 Flux partitioning using the AquaCrop model

2.2.1 AquaCrop model description

AquaCrop is a dynamic crop-growth model, which is used to predict the potential yields of herbaceous crops as a function of water consumption [59]. It is based on the approach developed in the FAO *Irrigation and Drainage Paper* No. 33 [60], which links crop water use and crop yield. The improvement brought to the FAO *Irrigation and Drainage Paper* No. 33 by AquaCrop is the separation between non-productive soil E and productive crop T. In this way, the biomass production is directly related to the productive part of ET through a productivity parameter [59]. This model combines four modules: (1) the atmosphere sub-model; (2) the crop development, growth, and yield; (3) the soil water balance; and (4) the management sub-model [61]. Only aspects related to the ET partitioning based on the reference ET will be detailed in the present work.

The model partitions ET into soil E (mm d^{-1}) and crop T (mm d^{-1}) at a daily timestep. According to [61], the crop T is given as:

$$T = K_s\left(CC^* \cdot K_{cTr,x}\right)ET_0 \quad (2.2.1)$$

where Ks (dimensionless) is the water stress coefficient, CC* (dimensionless) is the actual green canopy cover (CC) adjusted to consider micro-advective effects between the crop rows, $K_{cTr,x}$ (dimensionless) is the maximum standard crop T coefficient and ET_0 (mm d^{-1}) is the reference ET. Ks expresses the effects of water stress on diverse crop growth processes such as: (1) the slowing down of the canopy's expansion; (2) the stomata's closure; (3) the acceleration of the senescence; and (4) the modification of the harvest index (HI) after the beginning of the reproductive phase [61]. $K_{cTr,x}$ is adjusted by the model all along the simulation to consider the effects of ageing and senescence [62].

Soil E is described as [63]:

$$E = K_r(1 - CC^*)K_{ex}ET_0 \quad (2.2.2)$$

where K_r (dimensionless) is the E reduction coefficient and K_{ex} (dimensionless) is the maximum soil E coefficient. Kr expresses the reduction of E rate with the decrease in the soil water content in the

topsoil layer (defined as the first few centimetres of soil). This factor is equal to 1 during stage-I evaporation (when E is atmosphere-controlled) but drops below this value when the stage-II evaporation begins (when E is soil-controlled) [59]. K_{ex} can be adjusted depending on the management practices set up following the procedure described in the FAO *Irrigation and Drainage Paper* No. 56 [12].

AquaCrop considers three distinct growth phases for the computation of CC. As described in [59], the first phase starts at the emergence and ends when CC reaches the half of the maximum CC (CC_x). The equation associated to this phase is given as:

$$CC = CC_0 e^{CGC(t)} \tag{2.2.3}$$

where CC_0 (dimensionless) is the initial canopy cover of the soil and CGC(t) (dimensionless) is the canopy growth coefficient at a given time t. The CC_0 term results in the multiplication of the plant density by the mean canopy size per plant. This allows to consider the effect of plant density on canopy size [59]. The second phase is defined when 0.5*CCx < CC < CCx following the equation (2.2.4):

$$CC = CC_x - (CC_x - CC_0) e^{-CGC(t)} \tag{2.2.4}$$

The last phase is the senescence. During this growth phase, CC will decline until the time when no green canopy remains. This decline is characterized by an empirical canopy decline coefficient (CDC) [59].

The input variables required by the AquaCrop model are the following:

(1) Climatic inputs referring to: (i) maximum and minimum daily temperature (°C); (ii) daily precipitation (mm); (iii) daily reference ET (mm); and (iv) mean annual atmospheric CO_2 concentration (ppm).
(2) The crop parameters referring to: (i) planting date; (ii) emergence date; (iii) the date when the maximum effective rooting depth is reached; (iv) the date when the maximum green canopy cover is attained; (v) the date when the senescence starts; (vi) the date when the maturity is reached; (vii) the dates of the beginning and the end of the flowering; (viii) the maximum value of the $K_{cTr,x}$ coefficient; (ix) the maximum effective rooting depth; (x) the CC_0 and CC_x values; (xi) the CGC and CDC values; (xii) the productivity parameter value; (xiii) the reference harvest index (HI_O); and (xiv) the f_{HI} stress factor.
(3) The soil profile can be composed by a maximum of five layers. The inputs needed for each of these layers are: (i) the layer depth (m); (ii) the soil water content at field capacity (θ_{FC} in $m^3\ m^{-3}$), at the wilting point (θ_{WP} in $m^3\ m^{-3}$) and at saturation (θ_{sat} in $m^3\ m^{-3}$); (iii) the saturated hydraulic conductivity (K_{sat} in mm d^{-1}); (iv) the readily evaporable soil water (REW in mm); and (v) the curve number (CN).
(4) Depth (m) and salinity of the groundwater table if any.
(5) Parameters relative to the field management practices: (i) cover and type of mulching if any; (ii) practices relative to salinity; (iii) practices relative to soil fertility; and (iv) practices relative to the reduction of runoff.
(6) Parameters relative to the irrigation management practices: (i) irrigation method; (ii) irrigation scheduling data; (iii) irrigation depth; and (iv) salinity of the irrigating water.
(7) The initial condition at the simulation beginning, which are the initial soil water content and soil salinity in the soil profile.

AquaCrop features a user-friendly interface making its application simpler. Further information concerning the input variables and the concepts behind this model is available in the user manual of the AquaCrop software [61] and in the FAO *Irrigation and Drainage Paper* No. 66 [59].

2.2.2 ET_0 calculation

The calculation of ET_0 is required as it is an input variable of the AquaCrop model [61]. The equation applied was the Penman-Monteith equation described as follow [16], [17]:

$$ET = \frac{r_{CL,T}\Delta ED + \rho_a C_{ap} VPD}{r_{CL,T}\Delta + (r_{CL,L} + r_{can})\gamma} \quad (2.2.5)$$

where ET (here expressed in W m^{-2}) is the evapotranspiration, $r_{CL,T}$ (s m^{-1}) is the resistance to convective heat transfer, Δ (kPa K^{-1}) is the slope vapour pressure curve, ED (W m^{-2}) is the available energy, ρ_a (kg m^{-3}) is the air density, C_{ap} (J K^{-1} kg^{-1}) is the specific heat, VPD (kPa) is the vapour pressure deficit, $r_{CL,L}$ (s m^{-1}) is the resistance to convective water vapour transfer, r_{can} (s m^{-1}) is the canopy resistance and γ (kPa K^{-1}) is the psychrometric constant [16], [17].

As the reference ET is sought, some parameters are set to specific values. According to the FAO *Irrigation and Drainage Paper* No. 56, the reference crop is defined by an assumed height of 0.12 meters, canopy resistance of 70 s m^{-1} and albedo of 0.23 [12]. These values were therefore considered, notably for the aerodynamic resistance computation given as:

$$r_{CL,T} = \frac{1}{u.k^2}\left(ln\left(\frac{h-d}{z_0 m}\right) - \psi_m\right)\left(ln\left(\frac{h-d}{z_0 h}\right) - \psi_s\right) \quad (2.2.6)$$

where u (m s^{-1}) is the wind speed, k (dimensionless) is the von Karman constant, h (m) is the measurement height, d (m) is the zero-plane displacement height, z_{0m} (m) is the momentum roughness length, ψ_m (dimensionless) a function that takes into account the influence of atmospheric stability on the profiles established under neutral conditions adapted to momentum transfer, z_{0h} (m) is the sensible heat roughness length and ψ_s (dimensionless) is a function that takes into account the influence of atmospheric stability on the profiles established under neutral conditions adapted to sensible heat and water vapour[64]. Note that the relation linking $r_{CL,T}$ and $r_{CL,L}$ is:

$$r_{CL,L} = 0.93.r_{CL,T} \quad (2.2.7)$$

2.3 Flux partitioning using the Flux Variance Similarity approach

2.3.1 Conceptual overview

The Flux Variance Similarity (FVS) approach has already been described in details in Scanlon and Sahu (2008) and Scanlon and Kustas (2010). Since the FVS approach is based on the Monin-Obukhov similarity theory (MOST), it is necessary to establish the foundation by reviewing this theory first. The MOST [54] set that scalar statistics for a horizontally homogeneous atmospheric surface layer at a particular height are governed by: (1) the magnitude of the surface fluxes; (2) the surface shear stress; and (3) the buoyancy properties of the atmospheric turbulence [52]. A repercussion of this theory is that a perfect correlation should be observed between scalar time series measured at the same position [65]. Note that these conclusions are not always met under field conditions. Indeed, non-local phenomena and the heterogeneous distribution of sinks and sources can cause a violation of the assumption underlying the MOST ([53], [52]).

As carbon dioxide (c) and water vapour (q) concentrations are scalars, their high-frequency time series should exhibit a perfect correlation when measured at the same location. Note that the fluxes superposition of multiple source/sinks tends to degrade the overall correlation [66]. Let's

consider a case where T and photosynthesis are the sole contributors to the global carbon and water fluxes. As these processes are both stomatal, and thus occur at the leaf level, the correlation coefficient of their time series should be equal to -1 [53] since vegetation acts as a carbon sink but as a water vapour source. Another interesting characteristic of the relation between stomatal fluxes is that the slope of the photosynthesis-versus-T relationship is equivalent to the water use efficiency (WUE). This WUE is a leaf-level property, which links the amount of carbon dioxide gained per unit water loss by the plant [52]. Let's now consider a case where E and soil respiration are the sole contributors to the carbon and water fluxes. Assuming that, as the stomatal fluxes, the non-stomatal fluxes adhere separately to this FVS approach and since they are both positive during daytime, the correlation coefficient between these non-stomatal fluxes would be equal to +1 [52]. The Figure 2 from Scanlon and Kustas (2010) helps to visualise these relations [52].

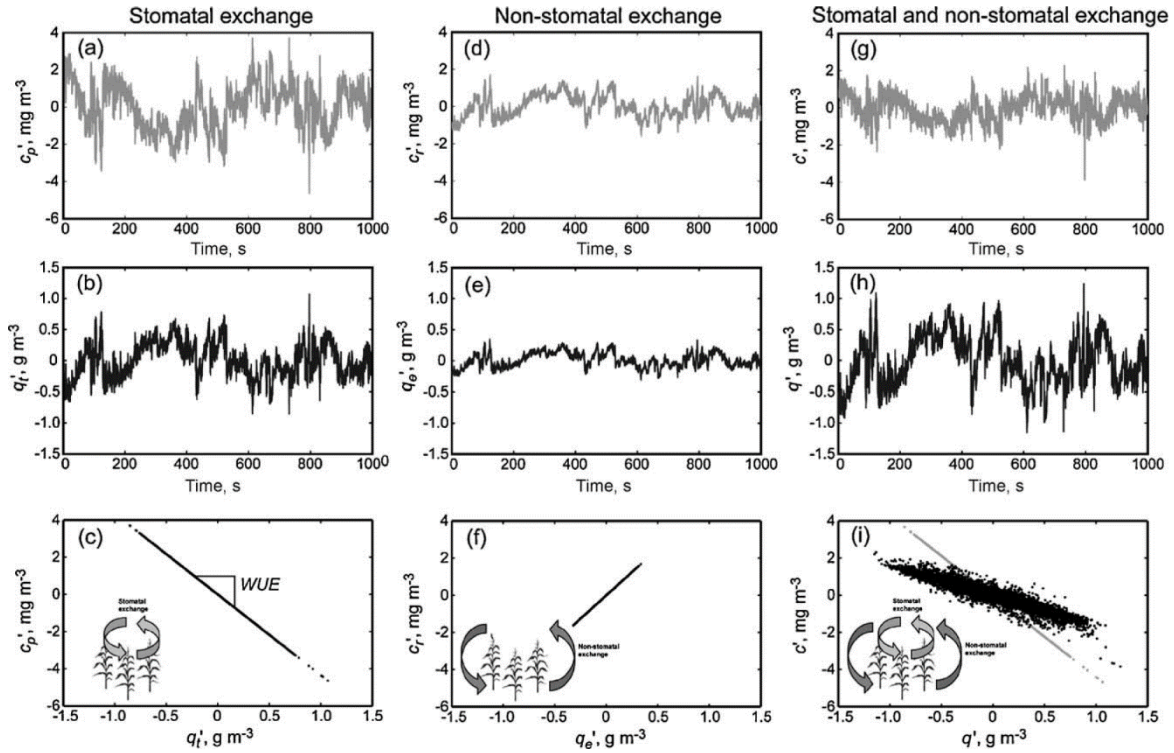

Figure 2 – High frequency time series of (a) carbon dioxide and (b) water vapour for a hypothetical case in which only stomatal exchange is active. (c) Flux-variance similarity applies to the stomatal exchange, implying perfectly negative correlation with a slope equivalent to the WUE of the vegetation. High frequency time series of (d) carbon dioxide and (e) water vapour for a hypothetical case in which only non-stomatal exchange is active. (f) Flux-variance similarity applies to the non-stomatal exchange, implying perfectly positive correlation. High frequency time series of (g) carbon dioxide and (h) water vapour for a more realistic case in which stomatal and non-stomatal exchange are both active. (i) The relationship between these time series exhibits less-than-perfect correlation with a slope deflected from WUE.

Let's finally consider a more realistic scenario where both stomatal and non-stomatal processes contribute to the carbon and water fluxes, a contamination of the perfect correlation exhibited by the stomatal fluxes by the non-stomatal fluxes should occur. The overall coefficient of correlation will therefore be higher than -1 [52]. The piece of information that can be derived from this correlation contamination is the relative magnitude of the flux's component.

The principle of the FVS approach consists in analysing the contamination degree of the correlation between stomatal and non-stomatal concentrations to infer the relative amount of the associated fluxes [66]. The outcome of the FVS method is the ET partitioning into E and T and the partitioning of the net ecosystem exchange (NEE) into photosynthesis and respiration.

2.3.2 Analytical approach

The first step of this analytical development is to decompose the vertical wind velocity (m s^{-1}), the water vapour concentration (kg m^{-3}) and the carbon dioxide concentration (kg m^{-3}) measured following the eddy-covariance method ([52], [67] and [66]):

$$q = \langle q \rangle + q' \tag{2.3.1.a}$$

$$c = \langle c \rangle + c' \tag{2.3.1.b}$$

$$w = \langle w \rangle + w' \tag{2.3.1.c}$$

where the $\langle\ \rangle$ and prime symbol stand for the temporal average of the water vapour concentration, carbon dioxide concentration and vertical wind speed over a short time interval (here 30 min) and the fluctuation from the mean value, respectively. The water vapour and carbon dioxide fluxes Fq and Fc (g m^{-2} s^{-1}) for this time interval are therefore given as:

$$F_q = \langle w'q' \rangle \tag{2.3.2.a}$$

$$F_c = \langle w'c' \rangle \tag{2.3.2.b}$$

These fluxes can also be expressed as a function of the stomatal and non-stomatal fluxes as follow:

$$F_q = F_{q_t} + F_{q_e} = \langle w'q_t{}' \rangle + \langle w'q_e{}' \rangle \tag{2.3.3.a}$$

$$F_c = F_{c_p} + F_{c_r} = \langle w'c_p{}' \rangle + \langle w'c_r{}' \rangle \tag{2.3.3.b}$$

where F_{q_t}, F_{q_e}, F_{c_p} and F_{c_r} (g m^{-2} s^{-1}) are the T flux, the E flux, the photosynthesis flux, and the respiration flux respectively, $q_t{}'$ and $q_e{}'$ (kg m^{-2}) are the stomatal and non-stomatal components concentration of the water vapour respectively and $c_p{}'$ and $c_r{}'$ (kg m^{-2}) are the stomatal and non-stomatal components concentration of carbon dioxide respectively [52].

In order to partition Fq and Fc into their stomatal and non-stomatal components, the following equations, formulated by Palatella, Rana, and Vitale (2014), need to be solved:

$$WUE\frac{\langle w'q' \rangle}{\langle w'c' \rangle}\left(\frac{\langle w'c_r{}' \rangle}{\langle w'c_p{}' \rangle} + 1\right) = \left(\frac{\langle w'q_e{}' \rangle}{\langle w'\ q_t{}' \rangle} + 1\right) \tag{2.3.4.a}$$

$$WUE\rho_{q,c}\sigma_q\sigma_c\sigma_{c_p}^{-2} = 1 + \frac{\langle w'c_r{}' \rangle}{\langle w'c_p{}' \rangle} + \frac{\langle w'q_e{}' \rangle}{\langle w'q_t{}' \rangle} + \rho_{c_p,c_r}^{-2}\frac{\langle w'c_r{}' \rangle \langle w'q_e{}' \rangle}{\langle w'c_p{}' \rangle \langle w'q_t{}' \rangle} \tag{2.3.4.b}$$

where:

$$\frac{\langle w'q_e{}' \rangle}{\langle w'q_t{}' \rangle} = -\rho_{c_p,c_r}^2 + \rho_{c_p,c_r}^2\sqrt{1 - \rho_{c_p,c_r}^{-2}\left(1 - \frac{W^2\sigma_q^2}{\sigma_{c_p}^2}\right)} \tag{2.3.5.a}$$

$$\frac{\langle w'c_r{}' \rangle}{\langle w'c_p{}' \rangle} = -\rho_{c_p,c_r}^2 \pm \rho_{c_p,c_r}^2\sqrt{1 - \rho_{c_p,c_r}^{-2}\left(1 - \frac{\sigma_c^2}{\sigma_{c_p}^2}\right)} \tag{2.3.5.b}$$

where WUE (kg CO_2 kg^{-1} H_2O) is the leaf-level water use efficiency, $\rho_{q,c}$ (dimensionless) is the correlation coefficient between the water vapour and carbon dioxide concentrations, σ_q and σ_c (kg m^{-2}) are the standard deviations of the water vapour concentration and carbon dioxide concentration over the time interval, respectively, $\sigma_{c_p}^2$ is the variance of the photosynthesis CO_2 concentration and ρ_{c_p,c_r} is the correlation coefficient between the photosynthesis and respiration CO_2

concentration. In these equations, five parameters are obtained from the eddy-covariance measurements (σ_q, $\rho_{q,c}$, σ_c, F_q and F_c) and three are unknown ($\sigma_{c_p}^2$, WUE and ρ_{c_p,c_r}). The WUE, which can be either measured or indirectly estimated, can be defined as:

$$WUE = \frac{\langle w'c_p' \rangle}{\langle w'q_t' \rangle} \tag{2.3.6}$$

This WUE value is crucial for solving the equations (2.3.4.a) and (2.3.4.b) with the remaining unknowns (i.e., $\sigma_{c_p}^2$ and ρ_{c_p,c_r}).

The flux components F_{c_p}, F_{c_r}, F_{q_t}, and F_{q_e} are then expressed as follow [52]:

$$F_{c_p} = \frac{\langle w'c' \rangle}{\left(\frac{\langle w'c_r' \rangle}{\langle w'c_p' \rangle} + 1\right)} \tag{2.3.7.a}$$

$$F_{c_r} = F_c - F_{c_p} \tag{2.3.7.b}$$

$$F_{q_t} = \frac{F_{c_p}}{W} \tag{2.3.7.c}$$

$$F_{q_e} = F_q - F_{q_t} \tag{2.3.7.d}$$

Importantly, the partition procedure may produce a valid result only when a set of conditions is fulfilled. Some conditions are set up to ensure the physical consistency of the algorithm, such as ([52], [66]:

$$F_{c_p} < 0 \tag{2.3.8.a}$$

$$F_{c_r}, F_{q_e}, F_{q_t} > 0 \tag{2.3.8.b}$$

$$-1 < \rho_{c_p,c_r} < 0 \tag{2.3.8.c}$$

$$W < 0 \quad when \quad \frac{F_c}{F_q} > 0 \tag{2.3.8.d}$$

$$W < \frac{F_c}{F_q} \quad when \quad \frac{F_c}{F_q} < 0 \tag{2.3.8.e}$$

Other conditions are set to ensure the mathematical consistency of the algorithm, i.e., the expressions in the root squares of both equations (2.3.5.a) and (2.3.5.b) must be positive [68]:

$$\rho_{c,q}^{-1}\frac{\sigma_c}{\sigma_q} \leq \frac{F_c}{F_q} < \rho_{c,q}\frac{\sigma_c}{\sigma_q} \quad when \quad \rho_{c,q} < 0 \tag{2.3.9.a}$$

$$\frac{F_c}{F_q} < \rho_{c,q}\frac{\sigma_c}{\sigma_q} \quad when \quad \rho_{c,q} > 0 \tag{2.3.9.b}$$

Scanlon, Schmidt, and Skaggs (2019) specified that these two last conditions are solely directed by the properties of the time series.

2.3.3 Fluxpart

Fluxpart (https://github.com/usda-ars-ussl/fluxpart.) is an open-source Python 3 tool that implements the FVS approach described previously. This module is fully described in a reference article

[66]. In addition to solving the algorithm, Fluxpart also applies basic QA/QC[3] to high-frequency eddy-covariance data and the external fluctuation corrections associated with temperature and vapour density ([69], [70]). Another interesting feature of the Fluxpart module is that it applies a wavelet decomposition to progressively remove the low frequency components of the data if no results has been found. The purpose of this filtering is to remove low frequencies that can degrade the relationships between the studied scalars by bringing non-local fluxes [53]. However, no spectral corrections are applied by Fluxpart.

Regarding the leaf-level water use efficiency, Fluxpart estimates this parameter with the following equation [66]:

$$WUE = 0.625 \frac{\langle c_a \rangle - \langle c_i \rangle}{\langle q_a \rangle - \langle q_i \rangle} \quad (2.3.10)$$

where c_a and c_i (kg m^{-2}) are the ambient and intracellular concentrations of carbon dioxide respectively and q_a and q_i (kg m^{-2}) are the ambient and intracellular concentrations of water vapour, respectively. The ambient concentrations of carbon dioxide and water vapour are estimated from the measurements and extrapolated at the leaf-level using a logarithmic mean profile [52]. The intercellular concentration of water vapour is equal to the saturation vapour pressure at the leaf surface temperature. To estimate the intracellular carbon dioxide concentration, a few options are available: (1) $\langle c_i \rangle$ can be considered as a constant value; (2) $\frac{\langle c_i \rangle}{\langle c_a \rangle}$ can be considered as a constant value; (3) $\frac{\langle c_i \rangle}{\langle c_a \rangle}$ can be expressed as a function (linear or square rooted) of the atmospheric vapour pressure deficit [71], or (4) $\frac{\langle c_i \rangle}{\langle c_a \rangle}$ can be determined based on an optimized model [68].

The variables playing a role on the parametrisation are the following:

- The leaf temperature. The model allows an external leaf temperature to be entered to improve the model performances. If no leaf temperature is given, the temperature considered is the sonic temperature computed from the raw eddy-covariance data.
- The hours of sunrise and sunset. If data is entered, the model will not try to partition fluxes from night-time. It will automatically assign the water vapour fluxes to E and carbon dioxide fluxes to respiration. If no data is given, the model will execute the partition even in night-time.
- The sub-model estimating the intracellular carbon dioxide concentration. No default sub-model is entered, it is compulsory to mention the sub-model used in the partitioning.
- The parameters linked to the sub-model estimating the intracellular carbon dioxide concentration. Default values are associated with each sub-model, but personalised values can be entered.

2.4 Evaluation of the simulations

2.4.1 Fluxpart's successful partition percentage

Only Fluxpart has been assessed regarding the percentage of half-hours successfully partitioned. As mentioned in the section 2.3.2, diverse conditions can lead to an unsuccessful partition. The no-results cases were counted and reported to the total number of filtered half-hours on a monthly basis. The term "filtered half-hours" refers to the half-hours filtered according to the footprint, the turbulence and the quality flag of the carbon dioxide and latent heat fluxes measurements. In addition, only daytime half-hours with no precipitation were considered as "filtered half-hours". The link

[3] Quality analysis and quality control. Refers to the detection of any metrological issues during the measures.

between the partition success and the atmospheric stability parameter was observed by means of boxplot.

2.4.2 Evapotranspiration

The performance of Aquacrop for ET prediction was assessed from the comparison between ET simulated values (i.e., E + T, equations 2.2.1 and 2.2.2) and values computed from eddy-covariance measurements.

Half-hourly turbulent flux values were filtered according to specific considerations of stationarity, footprint, and turbulence. Concerning the stationarity, only the good and intermediate quality flagged data was selected. With respect to the footprint, the half-hours with a maximum footprint greater than 200 m were not selected to only consider fluxes from the studied crop. This filtering produced gaps in the comparison dataset. As these gaps represented a loss of information regarding the cumulation of half-hourly data over a day, they needed to be gap-filled. This gap filling has been carried out using a random forest [72]. For this, $r_{CL,T}$, VPD, Δ and ED were considered as the explanatory variables of the actual evapotranspiration. The gap-filled half-hourly data was finally aggregated by day.

To compare the ET from eddy-covariance measurements and from AquaCrop simulation, several statistical indicators were chosen. The relative root mean square error (RRMSE), the coefficient of determination (R^2), the coefficient of efficiency (Eff) and the bias were used to compare the simulated and measured data [73], [74]. Eff is the ratio of the mean square error to the variance in the observed data, subtracted from unity [73]. This indicator can vary from minus infinity to 1, a higher value indicating better agreement. The bias is the mean of the difference between the simulations and the observations. A smaller bias expresses better predictions from the model.

These indicators were compared to the literature. The slope and the intercept of the predicted-versus-measured regression were also observed.

Note that a similar performance test for Fluxpart would be meaningless since Fluxpart-computed ET is, by definition, the turbulent flux. Numerical differences between the Fluxpart computation and full eddy-flux computation do exist but are only coming from incomplete correction applications applied by Fluxpart, and those missing corrections have no effect on the partitioning between E and T, which is the main goal of Fluxpart. In the following, only relative partitioned fluxes will be used from Fluxpart, and absolute partitioned fluxes will be computed using these fractions and the fully corrected turbulent flux.

2.4.3 Evaporation

The partitions processed by AquaCrop and Fluxpart were assessed by comparing the simulated E with the soil E predicted by the Beer's law [75], [76]. This law expresses the soil E as a fraction of the measured ET following this equation:

$$E = ETexp(-C.LAI) \tag{2.4.1}$$

where C (dimensionless) is the extinction coefficient of the vegetation and LAI (dimensionless) is the leaf area index. Following the method presented in [76], a log transformed based RMSE ($\ln(x+1)$) and the bias were calculated to compare these values of evaporation.

Note that the LAI was not measured on the study site. It is therefore the GAI (green area index) that was used to compute the Beer's law. The GAI was interpolated based on punctual measures, so this variable can contain errors. An additional point that one should be aware of is that the Beer's law

is a rough model approximation. Indeed, this model can only give an order of magnitude to expect for the simulated evaporation.

2.5 Models' comparison

The procedure applied to compare the AquaCrop and the Fluxpart models is the following and was inspired by the methodology developed in [77]. As the simulated ET fluxes were different between the two models, it was decided to base the comparison on the T/ET and E/ET ratios derived from both models. T and E values are therefore the T/ET and E/ET ratios calculated from the partition computed by each model multiplied by the ET measured by eddy-covariance. Note that this step is also necessary for Fluxpart even if ET is computed based on the raw eddy-covariance data. Indeed, since no spectral corrections are applied by Fluxpart as mentioned in section 2.3.3, the ET computed without corrections will be underestimated.

Now that the compared fluxes are consistent, there is still a time scale problem. Indeed, the AquaCrop model computes the partition on a daily timestep, but Fluxpart partitions ET on a half-hourly timestep. T and E simulated by Fluxpart thus each have to be summed daily, but since there are some gaps resulting from the conditions described in the section 2.3.2, these values have to be gap-filled first. This precaution is taken to avoid as much as possible a loss of information as explained in the section 2.4.2. Concerning the gap-filling, standard weeks were created based on weekly half-hourly binned diurnal cycles of T and E values [77]. The missing values were replaced by the corresponding typical half-hour values of the corresponding standard week. T and E derived from Fluxpart were then each summed daily and compared to T and E derived from the AquaCrop model.

2.6 Sensitivity analysis

In the absence of a reference, it was decided not to calibrate the two models. For AquaCrop, we believe that it is very well parametrised. Concerning Fluxpart, however, given (i) the small number of parameters, (ii) the uncertainty on these parameters, (iii) the impossibility of calibrating them, and (iv) the partition rates considered to be low, a sensitivity analysis was carried out on the framework of this study.

The sensitivity analysis carried out on the Fluxpart model was performed on three variables for one day:

- The c_i calculation option. The five proposed methods described in section 2.3.3 were compared.
- The constant-ratio value used in the case where the constant-ratio is selected to compute c_i. The values from 0.3 to 0.9 were tested in steps of 0.1.
- The temperature considered as the leaf temperature. Two temperatures were tested. The default temperature calculated by Fluxpart based on the eddy-covariance raw data (sonic temperature) and the canopy temperature measured on site using an infra-red sensor.

2.7 T/ET drivers' analysis

The study of the T/ET ratio drivers was conducted for AquaCrop and Fluxpart with the aim of comparing the link between the drivers and the ratio with both models. The studied drivers were the soil water content (SWC), the incident radiation (R), and the vapour pressure deficit (VPD). In order to estimate the correlation between the ratio and the drivers, a multiple regression was performed. Since T/ET is mainly conditioned by 3 variables, the study of the effect of only one of these variables on the flux has to be performed by fixing classes for the other two variables. The classes created for each driver are the following (Table 3 and Table 4):

Table 3 – classes dedicated to the study of the correlation between a single driver and the T/ET ratio for the Fluxpart partitioning.

Variable	Class 1	Class 2	Class 3	Class 4	Class 5
SWC	$SWC < 25$	$25 < SWC \leq 35$	$35 \leq SWC$	/	/
R	$R < 200$	$200 \leq R < 400$	$400 \leq R < 600$	$600 \leq R < 800$	$800 \leq R$
VPD	$VPD < 1$	$1 \leq VPD < 2$	$2 \leq VPD$	/	/

Table 4 - classes dedicated to the study of the correlation between a single driver and the T/ET ratio for the AquaCrop partitioning.

Variable	Class 1	Class 2	Class 3
SWC	$SWC < 25$	$25 \leq SWC < 35$	$35 \leq SWC$
R	$R < 150$	$150 \leq R < 250$	$250 \leq R$
VPD	$VPD < 0.5$	$0.5 \leq VPD < 1$	$1 \leq VPD$

The determination coefficient was then computed between the ratio calculated with both models and the associated driver as a function of the determined classes.

2.8 Canopy resistance computation

The equation used to compute the canopy resistance is the following [16], [17]:

$$r_{can} = \frac{r_{CL,T} * \Delta * ED + \rho_a * C_{ap} * D_a}{LE * \gamma} - \frac{r_{CL,T} * \Delta}{\gamma} - r_{CL,L} \quad (2.8.1)$$

which is a reformulation of the equation 2.2.5.

To compare the canopy resistance computed with ET ($r_{can,ET}$) and the canopy resistance computed with T ($r_{can,T}$), two calculations of the canopy resistance have been conducted. One replacing the LE term in the equation 2.8.1 by ET and one replacing this term by T derived from the Fluxpart partitioning. Only the Fluxpart partitioning was used because the daily timestep of the AquaCrop partitioning was not appropriate for a study of the canopy resistance. The aerodynamic resistance was calculated following the equation 2.2.6. The outliers were filtered by using the absolute deviation around the median (MAD) [78].

The comparison between these two canopy resistances was carried out during the period from April to August to only consider a period of well-developed vegetation. This period was divided into six sub-periods to observe the evolution of the bias and the percentage bias between $r_{can,ET}$ and $r_{can,T}$. The percentage bias and the bias were computed for each one of the sub-periods detailed in the table below (Table 5).

Table 5 - Start and end date of the sub-periods to study the time evolution of the bias.

Sub-period	1	2	3	4	5	6
Start date	01/04/2015	21/04/2015	12/05/2015	02/06/2015	23/06/2015	14/07/2015
End date	21/04/2015	12/05/2015	02/06/2015	23/06/2015	14/07/2015	02/08/2015

.

3 Results

3.1 Meteorological and phenological conditions

No drought episode was observed during this growing period. The temperature varied from - 5.8°C in Decembre to 32.6°C in July. Despite the sudden drop in soil water content during May and June, no edaphic drought is evident during this growing period The few gaps in the presented variables are due to brief malfunctions of the measuring equipment.

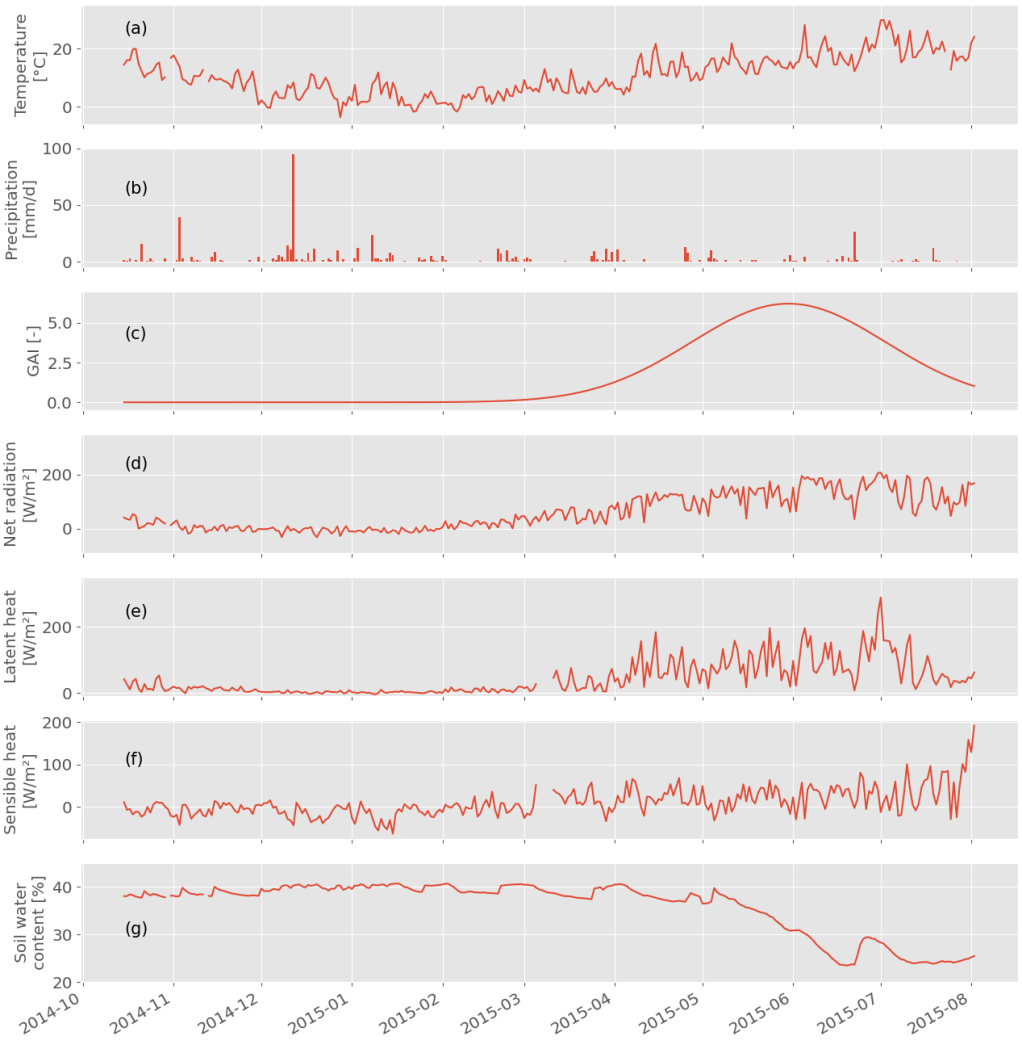

Figure 3 – Time evolution of the daily averaged meteorological and phenological variables over the cropping season with: (a) daily temperature average for the six hours around noon in °C, (b) daily precipitation in mm/day, (c) GAI (green area index) which is dimensionless, (d) daily net radiation average in W m^{-2}, (e) daily latent heat average in W m^{-2}, (f) daily sensible heat average in W m^{-2} and (g) soil water content (0.1 – 0.15 meter deep) in %.

3.2 Models' parametrisation

3.2.1 AquaCrop parametrisation

Regarding the crop parameters, a crop file created by Eline Vanuytrecht in 2009 especially adapted to winter wheat was used. The information concerning the duration of the different development stages, the maximum effective root depth, and all the conservative crop parameters (i.e., widely applicable crop parameters that do not require any local calibration) were not changed. But the plant density, the planting date, the crop decline coefficient, and the maximum canopy cover were adapted to this specific study. The maximum canopy cover value has been extracted from measurements data on winter wheat realized by the CRA-W during the 2014 – 2015 growing period on a site nearby Lonzee (Bordia).

Concerning the soil physical parameters, the values presented in Table 6 come from measurements carried out at the study site in the framework of another project. Note that no data were available regarding the saturation hydraulic conductivity. The default value of this parameter associated to a loamy soil was thus imposed, according to the AquaCrop default values. Regarding the initial soil water content, the values the day before the start of the simulation were used.

Table 6 - AquaCrop parametrisation.

Input variable	Value		
Climate: • Daily minimum and maximum temperature • Daily rainfall • Daily reference evapotranspiration	Calculated based on the meteorological measurements at the study site		
Crop parameters: • Planting date: • Plant density: • Maximum canopy cover: • Time to emergence: • Time to flowering: • Time to start of canopy senescence: • Time to maturity: • Maximum effective root depth: • Time to reach the maximum effective root depth:	14th of October 2014 183 plants/m² 84% 100 GDDays 1200 GDDays 1550 GDDays 2107 GDDays 1.5 m 1200 GDDays		
Soil physical parameters: • Θ_{Sat} (Soil water content at saturation): • Θ_{Fc} (Soil water content at field capacity): • Θ_{WP} (Soil water content at permanent wilting point): • K_{sat} (Saturation hydraulic conductivity):	0.0 – 0.20m 44.1% 37.3% 14.3% 50mm/day	0.20 – 0.55m 46.5% 39.9% 22.3% 50mm/day	0.55 – 0.85m 48.6% 42.9% 20.3% 50mm/day
Groundwater table: • Depth of the groundwater table:	Extracted from the measurements at the study site		
Parameters describing initial conditions at start of simulation period: • Initial soil water content at various depth in the profile:	0 – 0.05m 40%	0.05 – 0.15m 39%	0.15 – 0.25m 41%

3.2.2 Fluxpart parametrisation

These parameters (Table 7) were used to produce all the results presented in this chapter except those relative to the sensitivity analysis.

Table 7 - Fluxpart parametrisation.

Intracellular carbon dioxide concentration calculation method	Constant-ratio
Constant ratio value	0.7 (default)
Leaf temperature	Canopy temperature measured on site
Daytime	Hours of the sunrise and the sunset on site

3.3 Evapotranspiration measurements and modelling

In this section, only the AquaCrop ET simulation is investigated since the Fluxpart ET is computed on the same raw data than measured ET.

ET dynamics show two distinct periods (Figure 4). The first one covers October to April and is characterized by low temperatures and GAI, which lead to a low ET rate. The second one covers April to August and is characterized by higher temperatures and an increase in GAI, which also lead to an increase in ET rate. At the end of this second period, the crop senescence causes a decrease in the ET rate.

The comparison between AquaCrop-simulated and measured ET (Figure 4) associated with the bias value (Table 8) show that the simulated ET is globally overestimated. Regarding the RRMSE, its value is considered poor [74]. In contrast, R^2 and Eff are close to 1. This means on the one hand that the simulated flux dynamics are in good agreement with the measurements dynamics (Figure 5) and on the other hand that the model performance is considered as acceptable [73]. It would therefore appear that ET dynamics are well represented by the model, but that the predicted absolute values are not accurate.

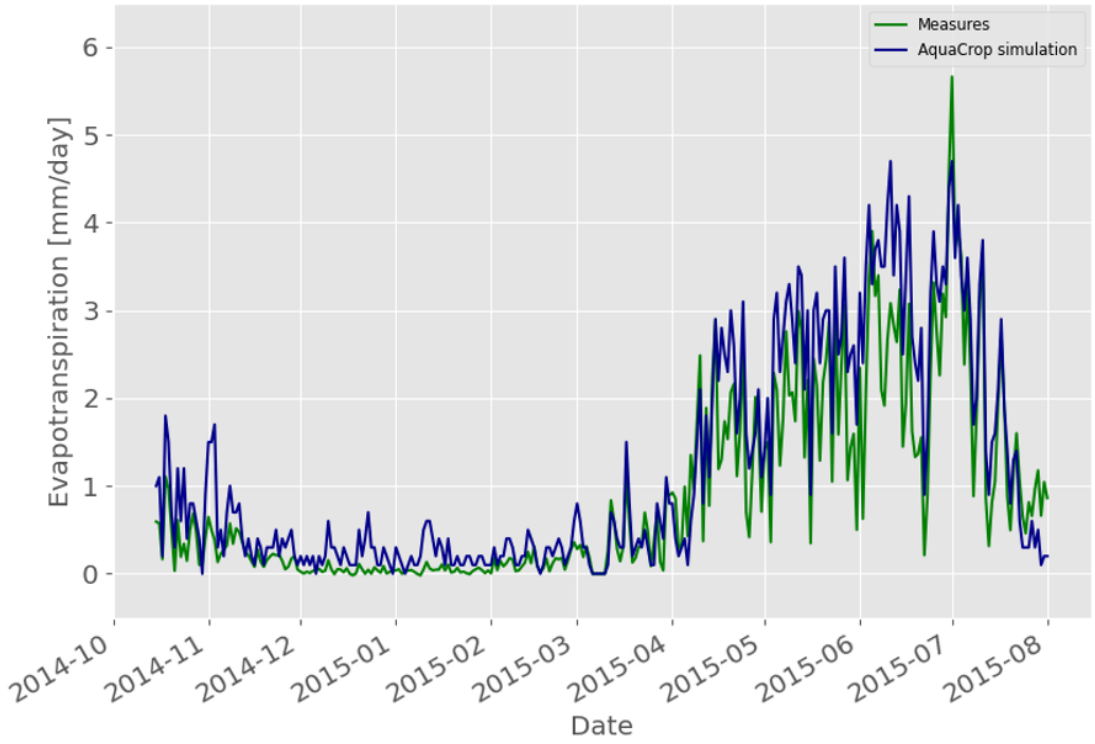

Figure 4 – Comparison between the evapotranspiration simulated with AquaCrop (blue line) and the measured evapotranspiration (green line) all along the growing period.

Table 8 - Statistical indicators of the comparison between the evapotranspiration simulated with AquaCrop and the measured evapotranspiration.

RRMSE	R^2	Eff	Bias
59.78%	0.94	0.755	0.295

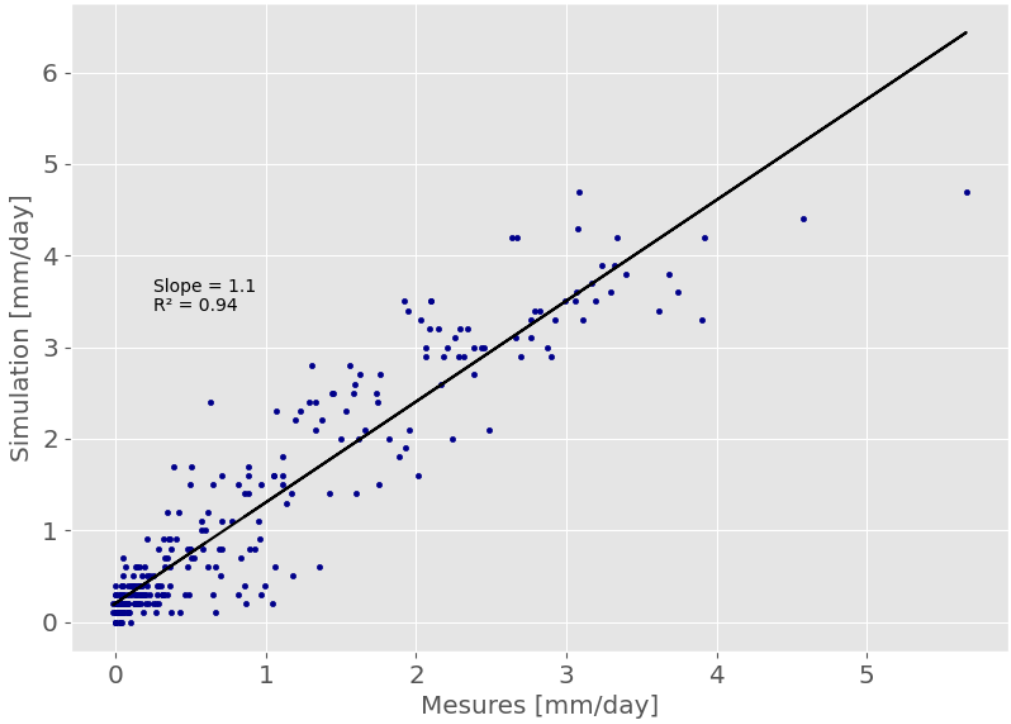

Figure 5 - Comparison between the evapotranspiration simulated with AquaCrop and the measured evapotranspiration.

3.4 Partitioning between evaporation and transpiration

As seen previously (Figure 4 and Figure 5), even if the ET dynamics are well reproduced by AquaCrop, the absolute values computed are significantly different from the measured ones. To compare the AquaCrop and Fluxpart ET partitioning, it has therefore been decided to extract the E/ET and T/ET ratios from both models and to apply them to the measured ET.

The overall dynamics of the ET partitioning between E and T are similar for the AquaCrop and the Fluxpart computations, with T dominating the water vapour exchange for the period starting in April (Figure 6 and Figure 7), consistent with the fact that the GAI is increasing rapidly at that time. However, strong differences can also be observed, with Aquacrop predicting a higher E fraction than Fluxpart during autumn and a lower E fraction from spring to harvest. As a reminder of the section 2.5, the gap filling is necessary to complete the time series relative to Fluxpart's partitioning to calculate the daily sums of the different studied fluxes (Figure 7).

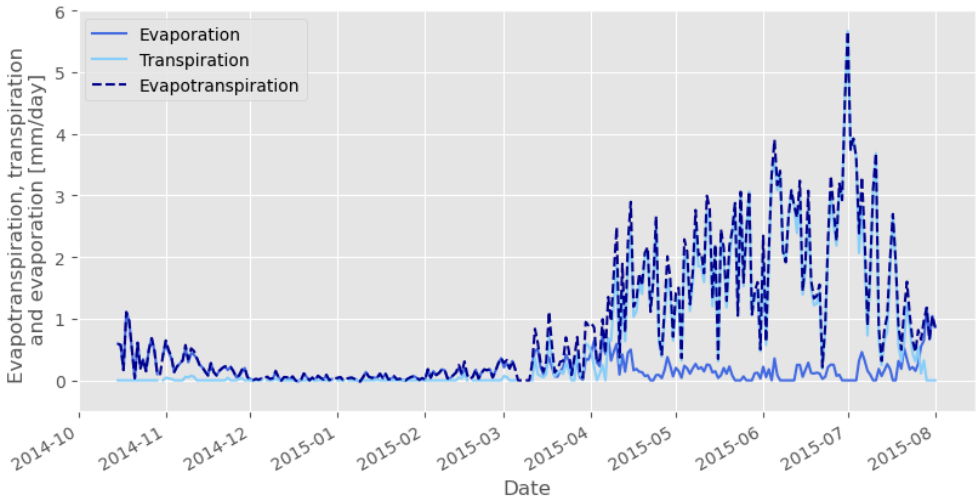

Figure 6 – Time evolution of the evapotranspiration partitioning between evaporation and transpiration computed with AquaCrop.

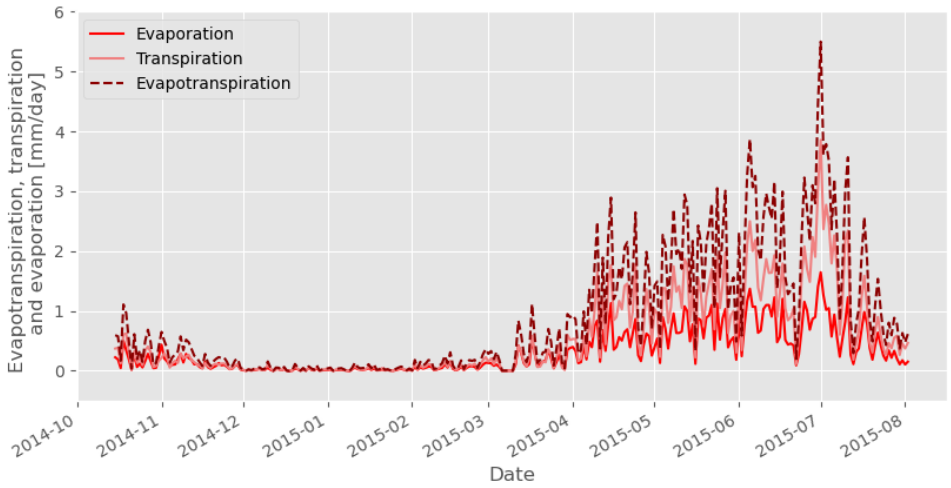

Figure 7 – Time evolution of the evapotranspiration partitioning between evaporation and transpiration computed with Fluxpart.

3.5 Statistics on the Fluxpart successful partition

The percentages of partition obtained (Table 9) were estimated very low compared to what could have been expected according to the literature [68]. So, it has been decided to put forward the study of the conditions in which the partition succeeds or fails. It appears that a determinant variable affecting the partitioning success could be the stability parameter. It was shown that the partition tends to fail more often in stable and neutral atmospheric conditions (positive and close to zero stability parameter) and to succeed more often under unstable conditions (negative stability parameter, typically below − 0.1) (Figure 8, Figure 9,Figure 10, Figure 11 and Figure 12).

Table 9 - Monthly partitioning percentage across the growing period. As a reminder of the material and method section, these percentages have been obtained by dividing the number of successfully partitioned half-hours by the number of "filtered half-hour" for each month.

Oct.	Nov.	Dec.	Jan.	Febr.	Mar.	Apr.	May	June	July	Aug.
30.08%	54.91%	47.64%	24.42%	51.96%	65.45%	48.32%	25.86%	31.46%	42.73%	7.14%

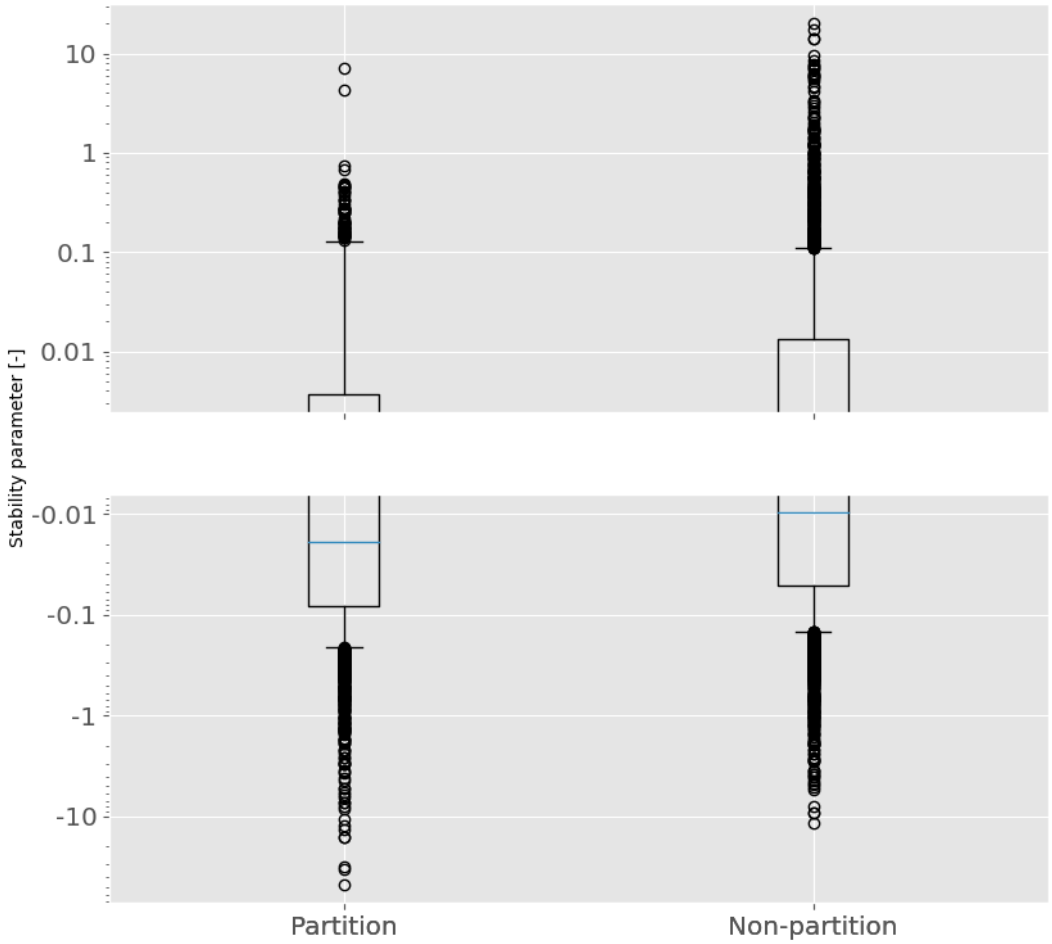

Figure 8 – Comparison of the stability parameter between the half-hours successfully partitioned and the half-hours for which Fluxpart failed to partition.

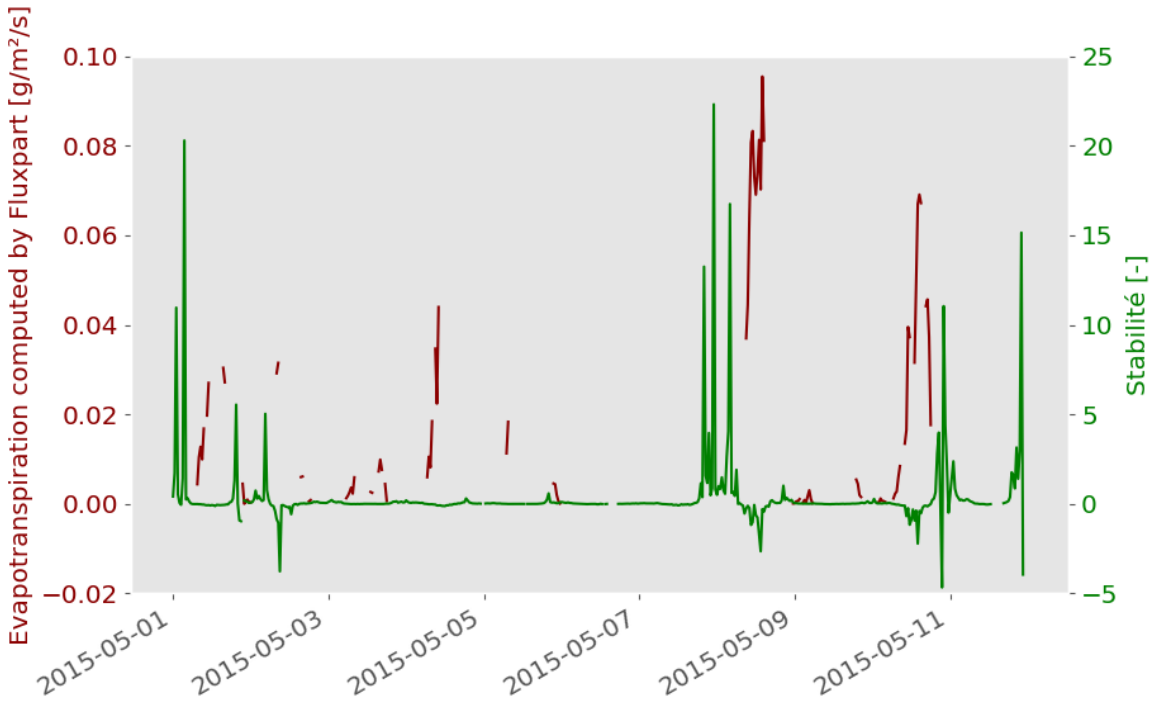

Figure 9 – Visualisation of the link between the success of the partition and the stability parameter for a period from the 1st of May to the 11th of May 2015. The evapotranspiration computed with Fluxpart is used as a visual indicator of the partitioning success.

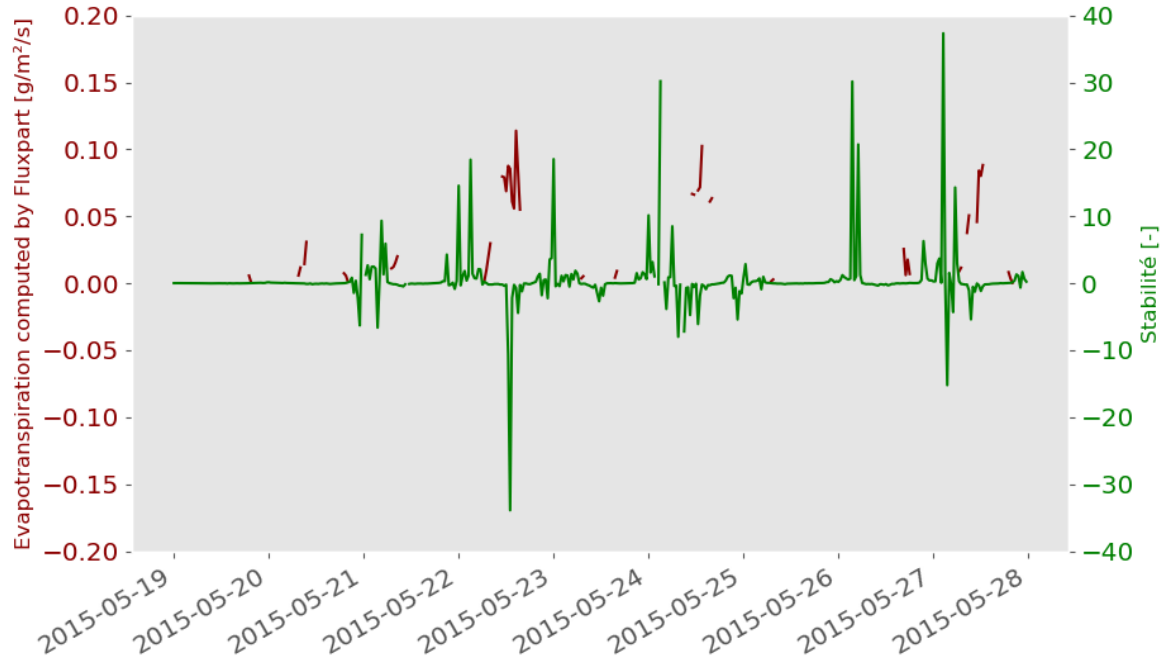

Figure 10 - Visualisation of the link between the success of the partition and the stability parameter for a period from the 19th of May to the 28th of May 2015. The evapotranspiration computed with Fluxpart is used as a visual indicator of the partitioning success.

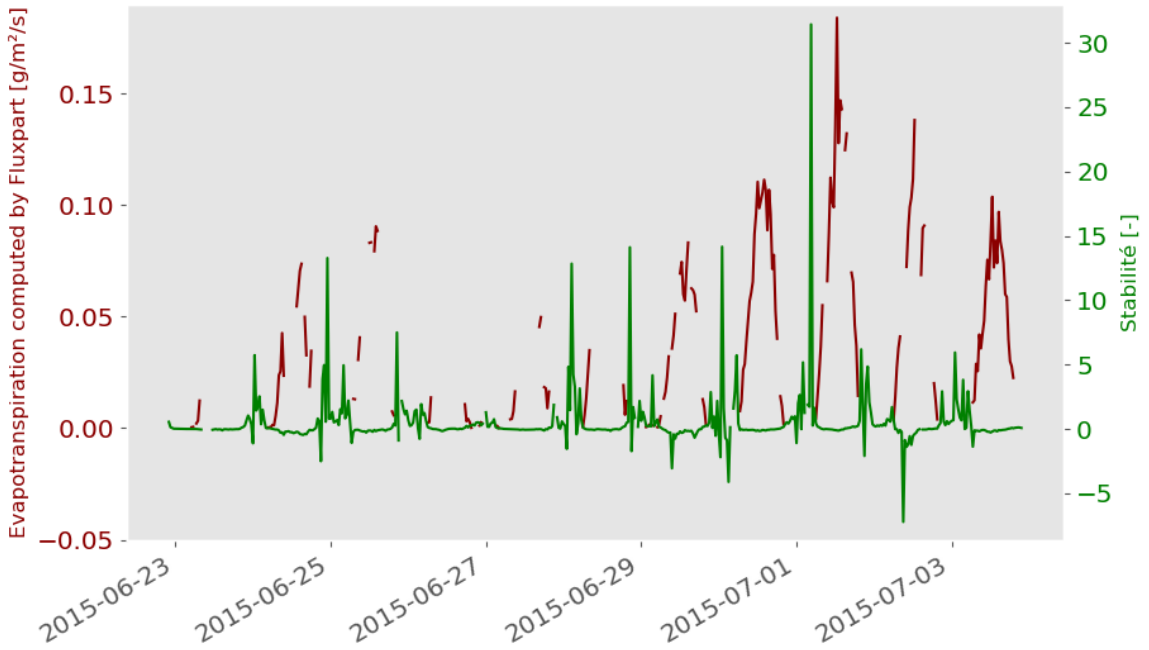

Figure 11 - Visualisation of the link between the success of the partition and the stability parameter for a period from the 23rd of June to the 3rd of July 2015. The evapotranspiration computed with Fluxpart is used as a visual indicator of the partitioning success.

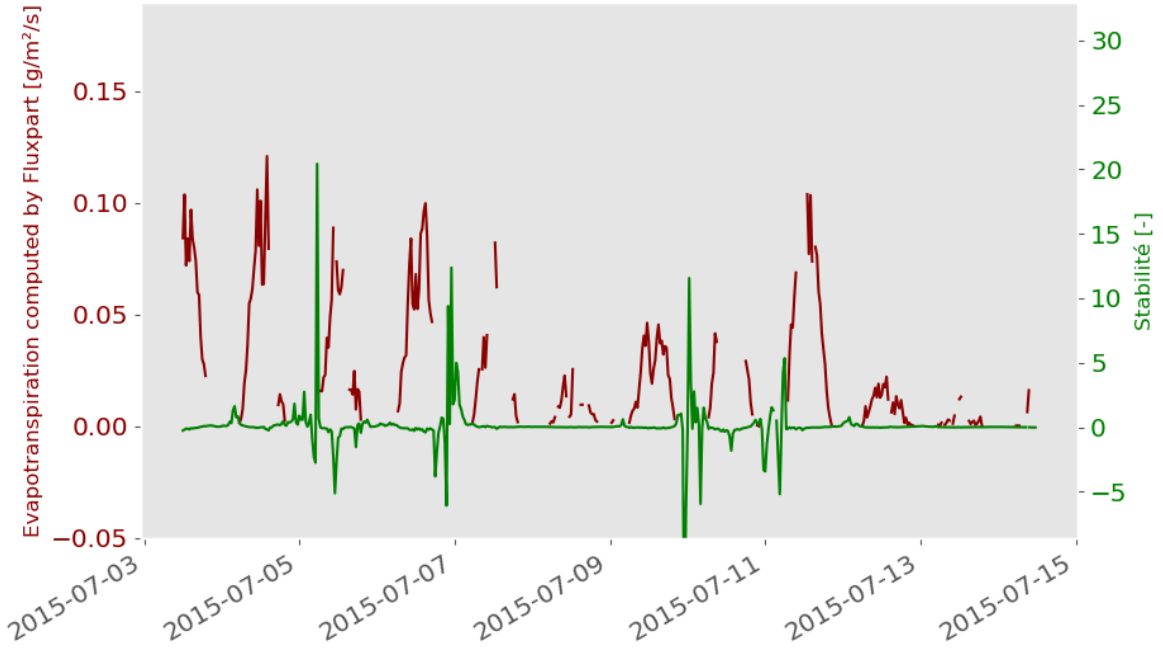

Figure 12 - Visualisation of the link between the success of the partition and the stability parameter for a period from the 3rd of July to the 15th of July 2015. The evapotranspiration computed with Fluxpart is used as a visual indicator of the partitioning success.

3.6 Sensitivity analysis (Fluxpart)

As a reminder of the material and method section, only Fluxpart is concerned by this sensitivity analysis. The day presented in the next part of the present section is the 17th of March 2015. This day was chosen because most of the day's fluxes were successfully partitioned.

Concerning the impact of the sub-model of c_i choice, the differences between the transpiration (T) computed with the various available computation methods are significant (Figure 13). T linked to the constant ratio and constant concentration are very similar. T linked to the squared root function of the VPD, and the optimization model are quite similar too, but T derived from the linear function of the VPD is different from the other one. All dynamics are similar, but the partitioning success is affected by the method chosen to compute c_i.

Regarding the influence of the constant ratio value on T, two observations can be made (Figure 14). The first one is that T increases with the constant-ratio value. This is logical because the WUE comes closer to 0 when the constant-ratio value increases (equation 2.3.10). The second observation is that the number of successfully partitioned half-hours is smaller for greater values of constant-ratio. This is due to the fact that, as mentioned above, the WUE approaches 0 when the constant-ratio value increases. This can lead to one of the partition conditions no longer being met (equation 2.3.8.e). The value imposed to the constant-ratio can thus also influence the partitioning success of the model.

Finally, concerning the input temperature, the T flux obtained with the default temperature (sonic temperature) is superior to the one obtained with the canopy temperature measured on site (Figure 15 and Figure 16). The dynamics between these two modalities are similar, that is an increase in T during the first half of the day and a decrease in T during the second part of the day. It is also interesting to note that the partitioning success seems affected by the temperature used for the model parametrisation.

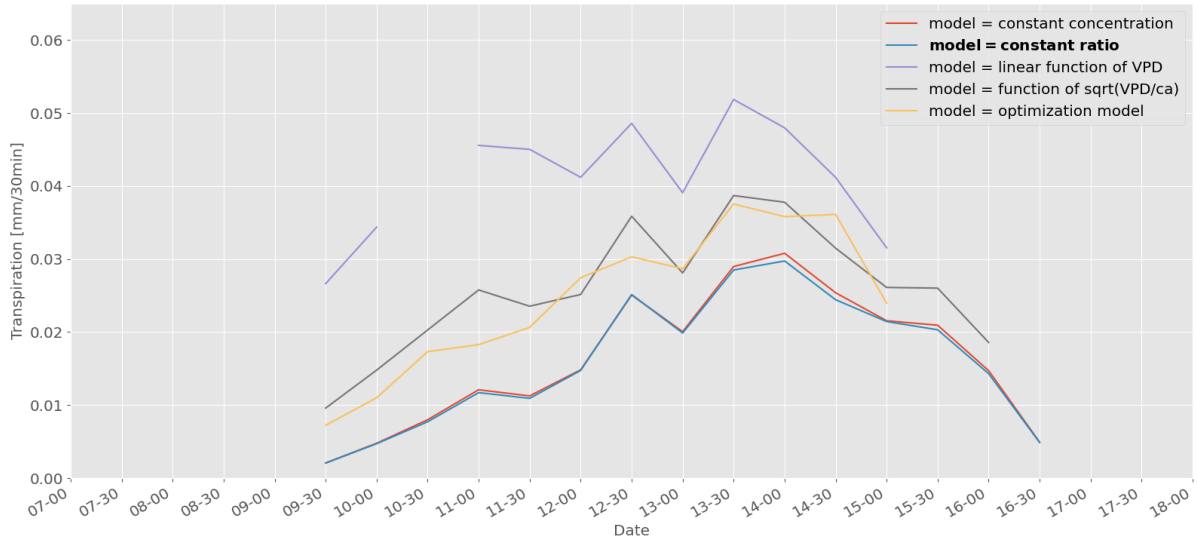

Figure 13 – Impact of the intracellular carbon dioxide concentration sub-model on the computed transpiration.

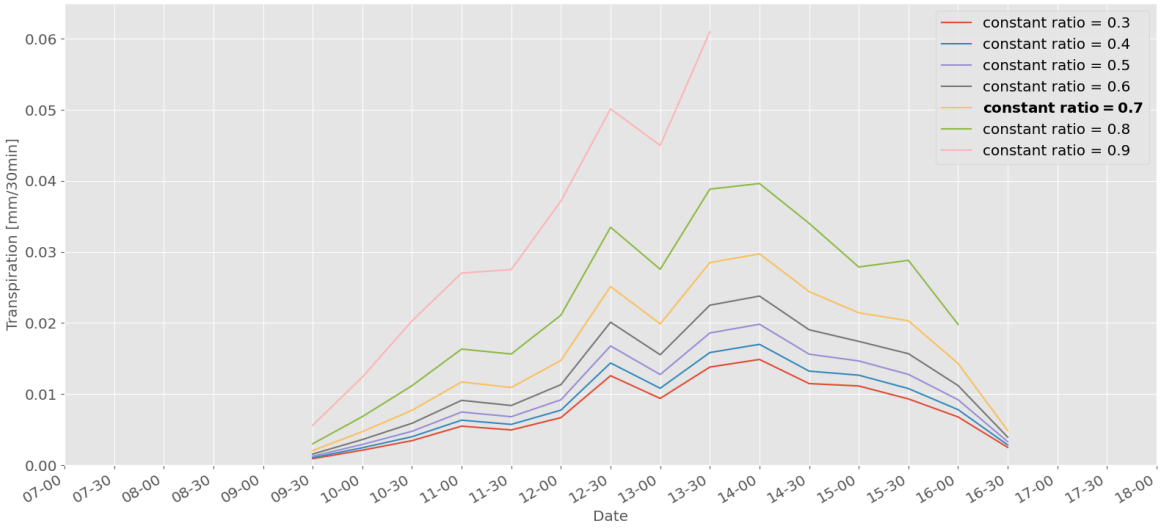

Figure 14 – Impact of the constant-ratio value on the computed transpiration.

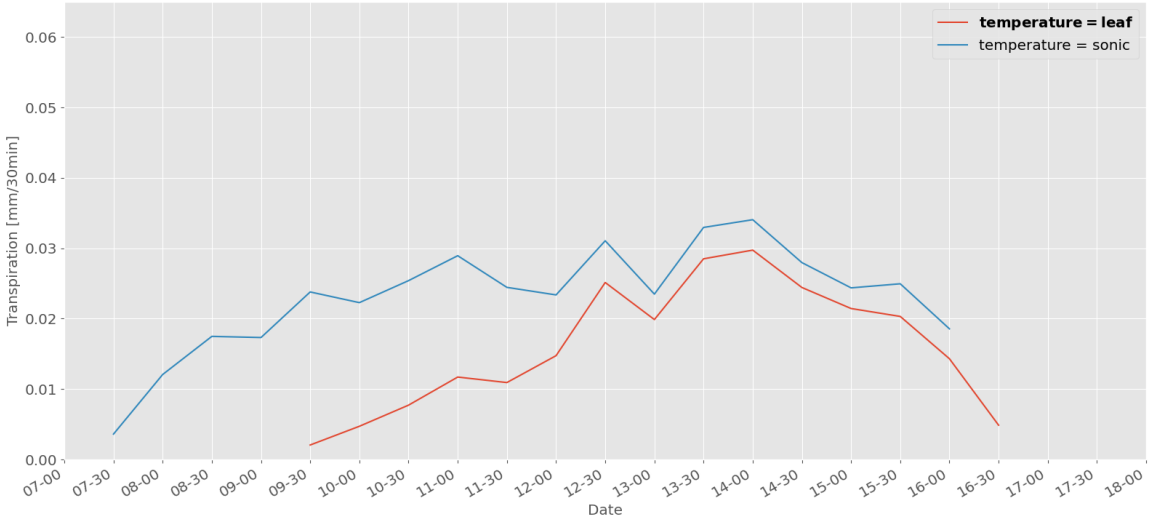

Figure 15 – Impact of the temperature (canopy or sonic) on the computed transpiration.

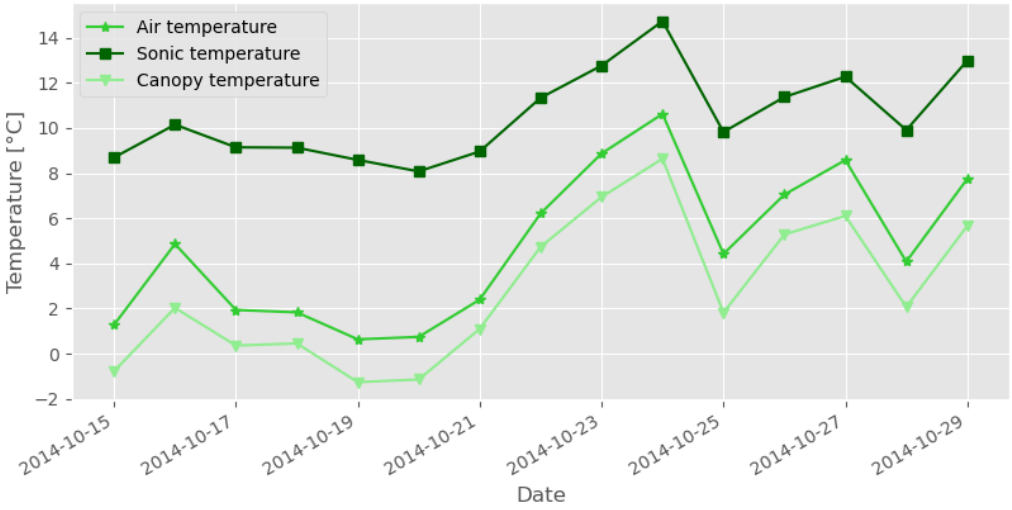

Figure 16 - Comparison between the daily mean sonic temperature (darkgreen), the daily mean air temperature (limegreen) and the daily mean canopy temperature (lightgreen) for the period from the 15th of October to the 29th of October 2014.

3.7 Partitioning validation based on the Beer's law

The AquaCrop predictions are in good agreement with the Beer's law predictions at the beginning of the growing period when the vegetation is not yet developed. But from March, some discrepancies appear between these two simulations (Figure 17). In contrast, E derived from Fluxpart differs from the one predicted with the Beer's law throughout the entire growing period. Indeed, on the one hand, Fluxpart underestimates E regarding the Beer's law for the period from October to May. But on the other hand, Fluxpart overestimates E regarding the Beer's law for the period from May to mid-July before the senescence starts. Note that E computed with Beer's law increases abruptly at the end of the growing period. This is due to the fact that the GAI is considered instead of the LAI. The GAI decreasing much faster than the LAI, the predict E is overestimated at the very end of the period. It is also noteworthy that E computed with AquaCrop also increases suddenly at the same period. This may be due to the fact that AquaCrop's partitioning is based on CC, but this will be addressed in more depth in the discussion of this work.

As mentioned in the section 2.4.3, E simulation has been assessed by computing the RMSEln and the bias for the comparison between E derived from AquaCrop and the Beer's law, the comparison between E derived from Fluxpart and the Beer's law and the values given in the reference article [76]. The RMSEln values from the comparison involving AquaCrop and Fluxpart are both in the interval presented in [76] (Table 10). Concerning the bias value, the absolute value of the Fluxpart model is also in the same interval as the one presented in [76]. But the AquaCrop's absolute value of the bias is slightly above the comparison interval. Also note that, contrary to what has been observed in the literature, the bias is negative. This expresses the fact that both AquaCrop and Fluxpart underestimate E regarding the Beer's law predictions.

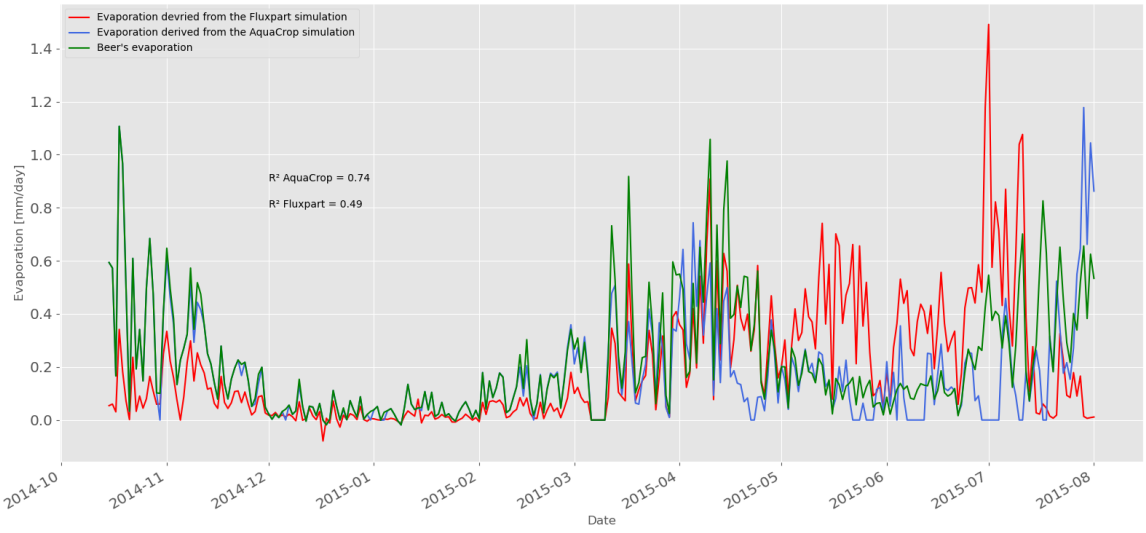

Figure 17 – Comparison between the evaporation predicted by the Beer's law (green), the evaporation derived from the AquaCrop simulation (blue) and the evaporation derived from the Fluxpart simulation (red).

Table 10 - Statistical indicators (log-transformed RMSE and bias) of the comparison of the evaporation simulated by AquaCrop and predicted with the Beer's law (blue part of the table), the evaporation simulated by Fluxpart and predicted by Beer's law(red part of the table) and the values presented in [76] (green part of the table).

AquaCrop		Comparison (Klosterhalfen)		Fluxpart	
RMSEln	Bias (W m^{-2})	RMSEln	Bias (W m^{-2})	RMSEln	Bias (W m^{-2})
1.77	- 61.59	[1:2]	[0:50]	1.27	- 34.71

3.8 Transpiration drivers' analysis

The following section presents the drivers analysis for both Fluxpart and AquaCrop models. Note that these models don't compute the partitioning at the same timestep. Indeed, the Fluxpart partitioning is at the half-hourly timestep and the AquaCrop model is at the daily timestep. The values presented in the tables below are thus computed based on half-hours for Fluxpart and on days for AquaCrop. This timescale difference not allowing a direct comparison, the AquaCrop's determination coefficients are mainly intended to present the expected order of magnitude for the link between the T/ET ratio derived from Fluxpart and the drivers. In this section, the links between the T/ET ratio and the VPD, the SWC and the R were studied. Basically, AquaCrop is supposed to present the reference determination coefficient as the partitioning is based on empirical relations. The period considered in this section is from April to mid-July to only consider well-developed vegetation period.

Considering the AquaCrop drivers' study, the determination coefficient of the multiple regression applied considering VPD, SWC and R as explanatory variables was 0.94. This means that the T/ET ratio is very well explained by these explanatory variables (Figure 18). Regarding the sub-classes' determination coefficient (Table 11), they are higher for the link between the T/ET and the VPD when SWC and R are fixed. Regarding the Fluxpart drivers' study, the determination coefficient of the multiple regression applied considering VPD, SWC and R as explanatory variables was 0.87. This also means that the T/ET ratio is well predicted by the explanatory variables (Figure 19). Note that the determination coefficient of the Fluxpart's driver analysis is smaller than the one computed based on the AquaCrop's drivers' analysis. Many features can cause that difference and they will be discussed in the next chapter. Finally, considering the comparison between the AquaCrop's drivers' analysis and the Fluxpart's drivers' analysis (Table 11 and Table 12), the sub-classes' determination coefficient are systematically smaller for Fluxpart than for AquaCrop whatever the variables fixed. Regarding the relation between T/ET ratio and SWC for fixed VPD and R, the determination coefficients are quite similar between the two models with AquaCrop's coefficients slightly higher. But the difference is greater for the relation between the ratio and R for fixed SWC and VPD and is even greater for the relation between the ratio and the VPD for fixed SWC and R, AquaCrop's coefficients always being higher than Fluxpart's ones.

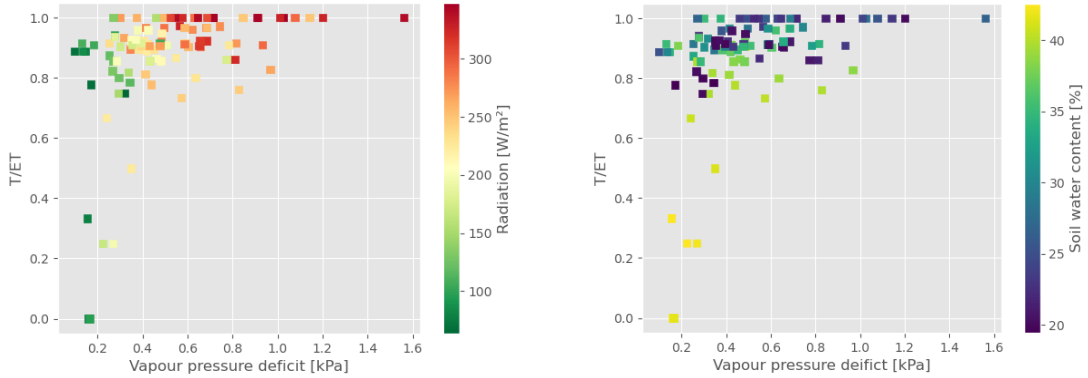

Figure 18 – AquaCrop drivers' analysis :(right) relation between T/ET ratio and the vapour pressure deficit as a function of the net radiation, (left) relation between T/ET ratio and the vapour pressure deficit as a function of the soil water content.

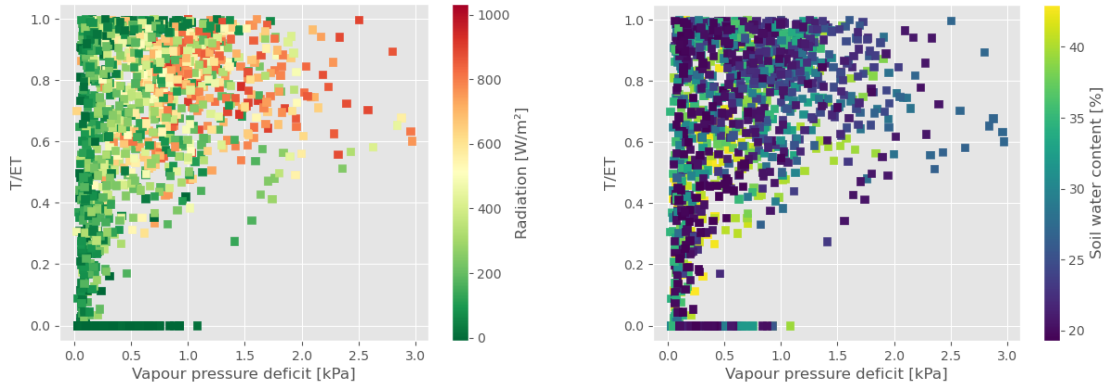

Figure 19 - Fluxpart drivers' analysis :(right) relation between T/ET ratio and the vapour pressure deficit as a function of the net radiation, (left) relation between T/ET ratio and the vapour pressure deficit as a function of the soil water content.

Table 11 - AquaCrop's drivers' analysis: study of the relation between T/ET ratio and SWC for fixed VPD and R (orange), study of the relation between T/ET ratio and R for fixed SWC and VPD (blue) and study of the relation between T/ET and VPD for fixed SWC and R (green). The "few data" on the table expresses that no or too little data was present in this category to compute a proper correlation analysis. The "" in the table indicates that data was available in this category, but all the T/ET ratios had the same value, making the correlation analysis impossible.*

R / VPD	1	2	3	SWC / VPD	1	2	3	R / SWC	1	2	3
1	53	58	39	1	62	34	82	1	93	11	36
2	Few data	67	27	2	32	82	95	2	48	80	55
3	Few data	Few data	*	3	*	*	Few data	3	81	81	97

Table 12 - Fluxpart's drivers' analysis: study of the relation between T/ET ratio and SWC for fixed VPD and R (orange), study of the relation between T/ET ratio and R for fixed SWC and VPD (blue) and study of the relation between T/ET and VPD for fixed SWC and R (green). The "few data" on the table expresses that no or too little data was present in this category to compute a proper correlation analysis. The "" in the table indicates that data was available in this category, but all the T/ET ratios had the same value, making the correlation analysis impossible.*

R / VPD	1	2	3	SWC / VPD	1	2	3	R / SWC	1	2	3	4	5
1	42	53	1	1	53	50	44	1	19	28	28	4	26
2	Few data	Few data	20	2	6	22	13	2	25	5	9	23	31
3	Few data	Few data	8	3	Few data	63	Few data	3	39	12	0.5	4	21

3.9 Consequences on canopy resistance estimations

In this section, only well-developed vegetation period was observed because other periods would not have been relevant. The temporal canopy resistance evolution shows that r_{can} decreases for the period from April to mid-May, stays low for the period from mid-May to the beginning of July and finally increases until the harvest (beginning of August) (Figure 20). In fact, the canopy resistance decreases when the GAI increases (Figure 21).

Regarding the differences between $r_{can,ET}$ and $r_{can,T}$, their percentage biases vary from 0.78% (thus negligible) for most of the month of June to 26.23% for the end of June and the beginning of July (Table 13). This is normal as T increases with GAI; thus, the T/ET ratio gets closer to 1 when the GAI increases. T getting closer to ET, the error made by approximating T and ET equality in the canopy resistance computation diminish with the canopy development. However, one should be aware that this analysis was conducted on gap-filled T data from Fluxpart computation. This gap-filling can thus bring some uncertainties in the evolution of the percentage bias across the compared periods. An example of this could be the jolt in the percentage bias observed during the third period (Table 13). Still, the bias computed is positive for each sub-class, meaning that $r_{can,T}$ is systematically superior to $r_{can,ET}$, which is consistent with the equation 2.8.1.

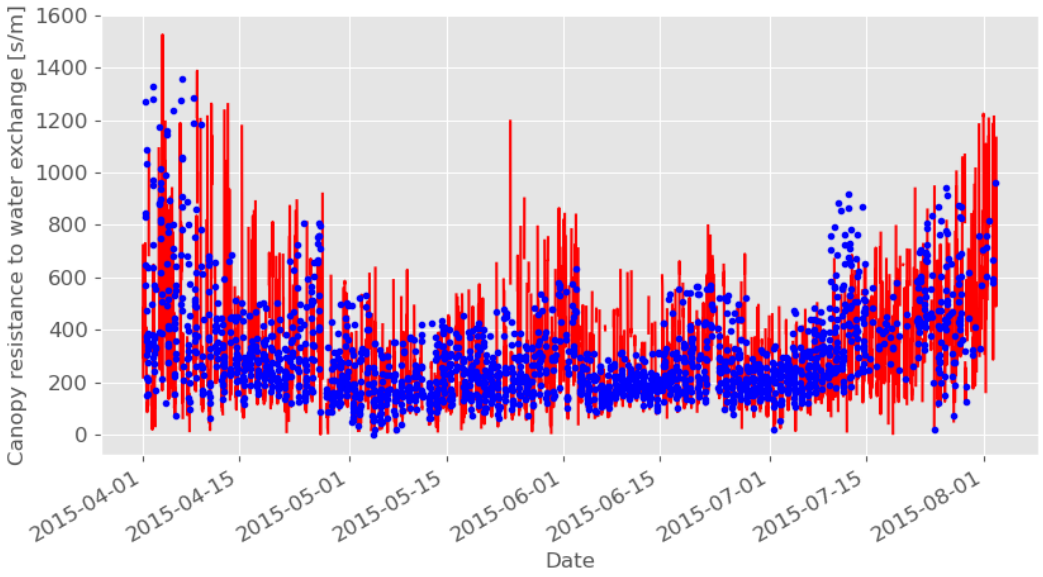

Figure 20 – Time evolution of the canopy resistance computed with the evapotranspiration (in red) and with the transpiration (in blue).

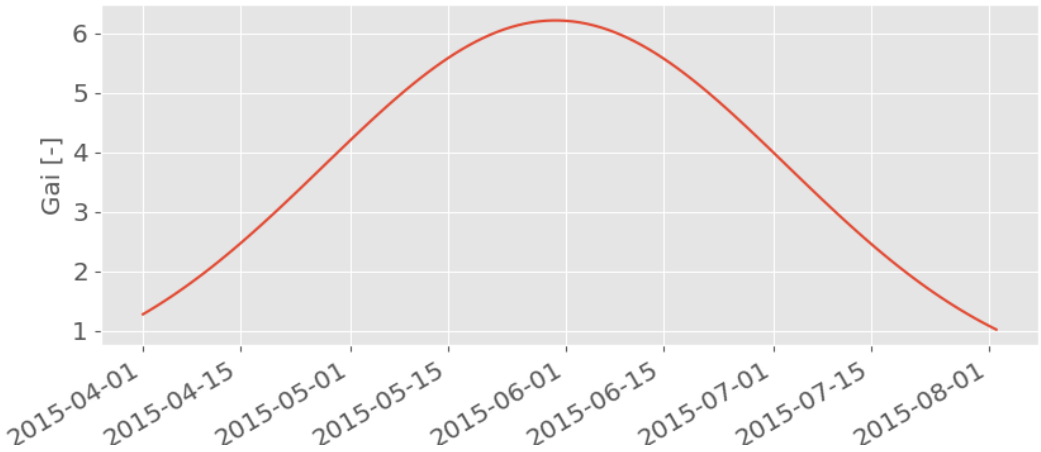

Figure 21 – Green index area for the period from April to the 2nd of August 2015.

Table 13 - Evolution of the bias and percentage bias between the canopy resistance computed with the evapotranspiration and with the transpiration over the well-developed vegetation period.

Sub-period	**1**	**2**	**3**	**4**	**5**	**6**
Percentage bias	4.59%	1.68%	8.82%	0.78%	26.23%	9.99%
Bias (s m^{-1})	24.87	5.46	34.87	3.11	82.5	142.16

4 Discussion and perspectives

4.1 ET partitioning computation

Before jumping into the discussion relative to the ET partitioning, a quick reminder of the general philosophy of the models used could be helpful. Firstly, AquaCrop is a crop-growth model based on soil water mass balance and empirical relations aiming to estimate the aboveground biomass produced during a growing period and the crop yield. To do so, the partitioning of the ET into E and T has to be conducted on a daily timestep. The domain targeted using this model is therefore agronomic. In contrast, the Fluxpart model relies on eddy-covariance raw data to partition not only water vapour fluxes, but also carbon dioxide fluxes at a half-hourly timestep. The partitioning computation follows the FVS theory that assumes that the scalars presenting collocated sources/sinks are perfectly correlated. The philosophy behind this model is mostly the comprehension of the fluxes exchange, no agronomic purposes are sought.

4.1.1 AquaCrop

According to numerous previous studies, the AquaCrop model has to be calibrated and validated before being applied. The usual calibrations are on CC, total soil water content, aboveground biomass and grain yield ([79]–[83]). None of these calibrations were carried out in the framework of this study for several reasons.

Firstly, no canopy cover measurements were available on site. Secondly, the calibration of the aboveground biomass and grain yield were beyond the scope of the present study. Indeed, as the objective of this work isn't the study of the AquaCrop's agronomical predictions, these variables were not used for any model's calibration or validation. Finally, regarding the total soil water content, the most accurate available information was used in the model. No calibration was therefore deemed necessary on this variable.

This absence of calibration and validation can degrade the AquaCrop's predictions regarding the partitioning of ET between E and T, notably through a misestimation of the CC (equations 2.2.1 and 2.2.2). Despite these warning signs, the partitioning computed by AquaCrop is still estimated reliable. Indeed, the crop file used in the framework of this study was specifically adjusted to winter wheat. This ensures that most of the non-conservative parameters (i.e., the parameters that require local adaptations) are relevant to the present situation. These are the reasons why, notwithstanding the absence of model calibration and validation, the model is considered to be well parametrised. Still, it is noteworthy that this absence of calibration and validation, notably regarding the CC, can be the cause of the overestimation of the simulated ET predicted by AquaCrop presented in Figure 4 and Figure 5.

4.1.2 Fluxpart

The use of Fluxpart is really convenient also because of the opensource software associated to this model [66]. This should allow to popularize this recent and complex method, which is beneficial given the many advantages of this model. Indeed, not only does Fluxpart partition the water vapour fluxes, but also those of carbon dioxide [52], [53]. In addition to this, the partitioning computation only relies on high-frequency raw eddy-covariance data and typical flux tower measurements, which makes it applicable in the majority of flux tower sites.

However, despite all these advantages, the number of successfully partitioned half-hours highlighted during this study was lesser than expected based on the literature [66]. As presented in the Figure 8, the partition failure mostly occurs during stable stability conditions. Regrettably, this study didn't manage to find any link between partition failure and mathematical conditions (equations

2.3.8; and equations 2.3.9). In addition to this, no publication concerning this model has so far mentioned such a problem, although their results were similar to ours (Graf, Klosterhalfen and Skaggs, personal communications). As this method is recent, there are still some grey areas.

Firstly, in Scanlon and Kustas (2010), they define the photosynthesis as "the gross ecosystem photosynthesis" and locate it at the leaf level. In the same article, they describe the respiration as the "total ecosystem respiration", they locate it at the soil level and add that this term regroups both heterotrophic and autotrophic respirations. As the term "gross ecosystem photosynthesis" refers to the gross primary production (GPP), this flux is supposed to represent only the plant's carbon dioxide uptake. But, following the definition of Scanlon and Kustas (2010), this term is supposed to be the sum of the photosynthesis and the aboveground autotrophic respiration (AAR). It would then mean that a part of the respiration is included in the photosynthesis term. Rather than the GPP, it would therefore be the net primary production (NPP) that is computed using the FVS theory. However, this would lead to inconsistency. Indeed, as the flux associated to the photosynthesis is the NPP, the CO_2 sources, which are associated with respiration fluxes, are distributed between soil (heterotrophic respiration and belowground autotrophic respiration) and leaf-level (aboveground autotrophic respiration). These are therefore not collocated anymore, which invalidates the assumption underlying the FVS theory. The assumptions that FVS computes notably GPP is then essential to apply this theory, but this means that the AAR is neglected. This flux being the dominant component of the respiration flux during the well-developed vegetation period [84], this approximation could cause an additional degradation of the contamination degree and thus distort the partitioning of the water vapour and carbon dioxide fluxes [52].

Then, a well-known problem of the eddy-covariance method is the lack of energy balance closure [85]. Indeed, the sum of the turbulent fluxes (latent heat and sensible heat) and the available energy (net radiation minus conduction) should typically be equal [86]. But it is rarely the case because of landscape heterogeneity, horizontal advection, metrological reasons, or a combination of these issues [85]. This problem is observed in almost every eddy-covariance site and the energy imbalance is approximatively 20% [85]. Concerning the present study, this percentage is 32%, which is superior to the values observed in previous studies [85], [87], [88].

Several interpretations are possible [89] :

- Either the available energy is overestimated, and the turbulent fluxes are correct;
- Or the turbulent fluxes are not perfectly measured because of advection phenomena or non-local events, and the available energy is correct.

The second hypothesis is retained. Indeed, with the increasing precision in the net radiation and conduction measurement, it is less likely that the imbalance comes from these variables [88]. This means that the turbulent fluxes are underestimated because of advection phenomena or low frequency eddies bringing away a part of the information. The ET and the resulting partitioning are also likely to be underestimated [87]. This could partly explain why the ET simulated by AquaCrop is superior to the one measured by eddy-covariance (Figure 4 and Figure 5).

This lack of closure in the energy balance can be due to two distinct processes. The advection and the presence of low frequencies on the study site. Considering the landscape surrounding the latter, no vertical advection is to be feared, but horizontal advection. The resulting horizontal displacement of air causes an information loss for the eddy-covariance measurement system. Considering the presence of low frequencies on the site, they also cause an information loss, but because of the size of the eddies. Indeed, the time interval of eddy-covariance measurement is 30 minutes, but some eddies can be larger than that. The information they contain therefore goes unnoticed and is not considered in

the energy balance. The presence of these low frequencies are imputable to a landscape heterogeneity [89]. The advection phenomenon is managed by only considering friction velocity above a certain threshold (here 0.1 m s^{-1}). But the low frequencies are tough to handle.

However, the Fluxpart model can filter low frequencies by applying a wavelet decomposition on the high frequency time series [66]. This allows to still consider half-hours presenting a low frequency content while respecting the conditions presented in equations 2.3.9.a and 2.3.9.b. So, there is a link between the partition success and the low frequency content on site. In addition to this wavelet decomposition, the friction velocity is filtered when the partitioning is computed. The partitioning will not even be attempted on half-hours with a friction velocity below the imposed threshold. This limits the risk of considering half-hours with strong advection phenomenon and thus limits the sources of non-valid root square to low frequency content mostly.

Low frequency content is then considered to be linked with both partitioning success and energy balance. It is interesting to note that a previous study showed a link between the lack of energy balance closure and both stability parameter and friction velocity [88]. They proved that the energy balance deficit is more important for stable and neutral stability conditions and for smaller friction velocity [88]. Their observations concerning the link between the stability parameter and the energy imbalance seem similar to the insights presented in Figure 8, Figure 9, Figure 10, Figure 11 and Figure 12. It would therefore be interesting to further research in this direction to evaluate if the partition success follows the same pattern. This would not only allow to better understand the link between the stability parameter and the partitioning success, but also to better predict the periods and sites in which the partitioning is likely to be less successful.

Another point that is important to address regarding Fluxpart is the sensitivity analysis, which was conducted on three distinct variables, namely the intracellular carbon dioxide concentration sub-model, the value chosen for the constant-ratio and the temperature (see section 2.6). Firstly, concerning the sensitivity analysis relative to the choice of the sub-module computing the intracellular carbon dioxide concentration, it was showed that some sub-models are quite similar while others are clearly different (Figure 13). Similarities between the constant concentration sub-model and the constant ratio sub-model when their default values are considered is quite logical. Indeed, the default value for the constant-ratio sub-model is 0.7 and for the constant concentration, it is 270 ppm. The ambient concentration of carbon dioxide being around 385 ppm, 70% of this concentration gives us the constant-concentration default value. This explains the similarities between these sub-models. Two others sub-models are also quite similar. It is the optimization sub-model and the squared rooted VPD sub-model. This is probably due to the likeliness of these sub-models governing equations (equation 4.2.1 and equation 4.2.2).

$$\frac{ci}{ca} = 1 - \sqrt{\frac{1.6 * \lambda * VPD}{ca}} \tag{4.2.1}$$

$$\frac{ci}{ca} = 1 - \frac{\sqrt{a\overline{VPD}m * (\overline{ca} + a\overline{VPD}m)} - a\overline{VPD}m}{\overline{ca}} \tag{4.2.2}$$

They both adhere to an expression depending on the squared root of the VPD. Finally, the last sub-model is the linear model, which relies on a linear relation between the ci/ca ratio and the VPD. It is clearly different from the other models and tends to predict a way higher T than the other sub-models. Despite such significant differences between the proposed sub-model, none of them are unanimously accepted through the scientific community. Further research could therefore by handled in this

direction by comparing actual T and E measures with the Fluxpart predictions to establish the more accurate sub-model to use.

Secondly, concerning the value chosen for the constant-ratio, the higher this value, the higher the T computed (Figure 14). This is also explicable via the observation of the equation 2.3.10. Indeed, the ambient carbon dioxide concentration being always superior to the intracellular carbon dioxide concentration, the numerator of this expression will always be positive. The denominator of this expression is always negative because the intracellular water vapour concentration is always superior to ambient water vapour concentration. The higher the numerator, the more negative is the WUE and a more negative WUE means a lower T. A higher numerator meaning a small ci/ca ratio, a small ci/ca ratio induces a lower T while a higher ci/ca ratio induces a high T. This is consistent with the curves presented in Figure 14. This reasoning allows to suspect that the linear sub-model predicts a higher ci/ca ratio while the constant-concentration and the constant-ratio sub-model predicts smaller values for this ratio. The realization of this sensitivity analysis allowed the disclosure of a mistake in the source code of Fluxpart. This error, preventing any manually entered sub-model values from being considered, was corrected in the framework of this sensitivity analysis.

Finally, concerning the sensitivity analysis relative to the temperature, it was presented (Figure 15) that the transpiration (T) computed using the sonic temperature was higher than the one computed with the leaf temperature. This is because a higher temperature will cause a higher intracellular water vapour concentration (qi) in leaves. A higher qi will cause a less negative WUE and finally a more important T (equation 2.3.7.c). In contrast, lower temperatures would cause a more negative WUE then a smaller T. This was already observed in [76]. The leaf temperature almost always being cooler than the sonic temperature (Figure 16), the T computed with the leaf temperature will always be inferior to the T computed with sonic temperature. Note that the partitioning results are significantly different when the leaf temperature (0.015 mm/30min +- 0.009) or the sonic temperature (0.022mm/30min +- 0.009) is considered. Assuming that the leaf temperature and the sonic temperature are equal thus leads to a significant T overestimation. Yet this is often seen in previous studies [52], [66]–[68], [90]. It is then important to be aware of the bias brought by not using the leaf temperature. Some advice would be, to enter an air temperature even if the leaf temperature is not measured on a site. This is because the air temperature is always higher than the leaf temperature but is still lower than the sonic temperature (Figure 16). This would lead to a limited bias and thus to a limited T overestimation.

Note that the choice of intracellular carbon dioxide concentration sub-model, constant-ratio values or temperature also affect the partitioning success. Indeed, as mentioned before, some conditions are imposed to ensure the mathematical consistency of the algorithm (equation 2.3.9.a and equation 2.3.9.b). These conditions express that when the WUE is less negative, the risk of no longer meeting this condition is greater. This means that each choice that prefers an option that computes a less negative WUE will have a greater chance of not respecting the existence conditions of the algorithm. It is visible in the Figure 13 (with the linear model achieving less partitioning than the optimized and the squared rotted sub-models, themselves leading to less half-hours successfully partitioned than the constant-concentration and the constant-ratio sub-models), Figure 14 (with higher ci/ca ratio values leading to less half-hours successfully partitioned), and Figure 15 (with higher temperature leading to a reduced number of partitioned half-hours).

A final comment on the application of Fluxpart is that it has been shown that the performance of this model is better when there is an important spatial separation between the sources and sinks of water vapour and carbon dioxide [76]. This model should then present better performances when applied on forest ecosystems. Although we are in an agricultural ecosystem, this model was still

considered adapted considering previous studies that used Fluxpart under conditions similar to those in this study [76], [77], [91].

4.2 Comparison of the partitioning methods

First of all, it is noteworthy that both models partition ET following the same general dynamics (Figure 6 and Figure 7). These general dynamics show a dominance of E in winter when the vegetation is not yet developed, a gradual increase in the proportion of T as the vegetation develops and finally a dominance of T when the vegetation is well developed [92], [93]. One should note that, unlike AquaCrop, the link between vegetation development and water vapour flux partitioning does not appear in the Fluxpart's construction. The adherence of Fluxpart to these well-established dynamics is then quite reassuring.

However, significant differences were still found (Figure 6 and Figure 7). It is possible to observe three distinct phases during the growing period:

- From October to mid-March: the AquaCrop's E was superior to Fluxpart's E. In other words, Fluxpart's T predictions are higher than AquaCrop ones. This is probably due to the presence of weeds on the field. Indeed, weeding practices had to be conducted on the field during this period, which expresses the presence of weed that was not considered in the AquaCrop simulation.
- From mid-March to the end of July: the Fluxpart's E was superior to AquaCrop's E. This may be due to the negligence of the AAR in the Fluxpart model that was already discussed in section 4.1.2, this causing a T underestimation.
- From the end of July to the 2nd of August: the AquaCrop's E was superior to the Fluxpart's E. This period corresponds to the end of the crop senescence. During this period, the green canopy cover decreases dramatically because of the crop's yellowing. But even if no green canopy remains, the yellowed vegetation still mitigates the evaporation flux through shading. The reason why AquaCrop predicts a way more important E than Fluxpart is because its ET partitioning is based on the green canopy cover (equation 2.2.1 and equation 2.2.2) and as CC decreases, E increases.

Now that such differences have been identified, it is natural to ask which model is the best or the most efficient. To answer this question, a look back at sections 2.4.3 and 3.7 is necessary. The values presented in Table 10 showed that the log-transformed RMSE computed between the Beer's law's E and the Fluxpart's E is smaller than the one computed between the Beer's law's E and the AquaCrop's E, although they are in the same interval than the log-transformed RMSE presented in the reference article [76]. This table shows that Fluxpart's E predictions are closer the ones computed with the Beer's law than the AquaCrop ones. This observation is also valid regarding the bias value. Indeed, the Fluxpart's bias being smaller than the AquaCrop's bias, the mean difference between simulations and observations is smaller for Fluxpart predictions. One might therefore think that Fluxpart performs better than AquaCrop. But when the determination coefficient is computed between the E calculated with Fluxpart and the Beer's law on the one hand, and the E computed with AquaCrop and the Beer's law on the other hand, the determination coefficient of the relation involving AquaCrop is the highest. This means that AquaCrop's E prediction dynamics are more similar to the Beer's law one than the Fluxpart one. It is therefore hard to determine the most accurate model as Fluxpart predicts better absolute values and AquaCrop predicts better dynamics.

It is still very difficult to decide which model is the best since only one validation was computed in the framework of this study. This is a weak point of this work. However, this study is not the only to suffer from a lack of validation for water vapour fluxes partitioning [7]. Note that other validation

methods exist for Fluxpart, but they would involve the consideration of the carbon dioxide flux partitioning, which is out of the framework of the present study.

Concerning more specifically the validation method used, it could be improved by measuring an actual extinction coefficient. Indeed, the extinction coefficient is adapted as much as possible to the crop [94], but still presents uncertainties which it is impossible to quantify with the available measures. This validation method could then be improved. This improvement could be done by installing a pyrradiometer below the canopy to measure the amount of radiation passing through the crop canopy and reaching the soil surface. This way, no uncertainties would be linked to the extinction coefficient anymore.

A last point that is interesting to address concerning the comparison of the partitioning methods is the link they have with their drivers (Figure 18, Figure 19, Table 11 and Table 12). The determination coefficient of the AquaCrop's multiple regression is higher than the one related to Fluxpart. This means that AquaCrop partitioning is more related to the explanatory variables than Fluxpart. As a reminder, the explanatory variables were the vapour pressure deficit (VPD), the soil water content (SWC) and the net radiation (R). The analysis of the sub-classes' determination coefficient allowed to highlight the fact that AquaCrop's determination coefficients for the relation between the T/ET ratio and the VPD for fixed R and SWC were significantly higher than the Fluxpart's ones. This means that AquaCrop is more linked with the VPD than Fluxpart. This finding can also be made to a lesser extent with the link between the T/ET ratio and the SWC for fixed R and VPD. It would therefore appear that not only AquaCrop partitioning is more related to the VPD, the R and the SWC in general than Fluxpart, but also that AquaCrop partitioning is more linked to the VPD and the SWC than Fluxpart. This may be due to the fact that the Fluxpart's partitioning is affected by some approximations (see section 4.1.2). Further study of the link between partition methods and their drivers could be conducted by considering, for example, shorter periods centred on episodes of large divergence between the model's predictions.

4.3 Partitioning impact on the canopy resistance

Usually, the canopy resistance is computed by approximating that the T is equal to the ET, which is only the case when the vegetation is well-developed. A previous study said that this approximation can be made if the leaf area index (LAI) is higher than 4 but should be considered with caution for less dense canopies [95]. Although the LAI wasn't measured on the study site, the same observations were carried out based on the green area index (GAI) measurements. By considering the results advanced in the section 3.9 (Figure 20, Figure 21 and Table 13), the comparison with the conclusions drawn in previous study can be made [95].

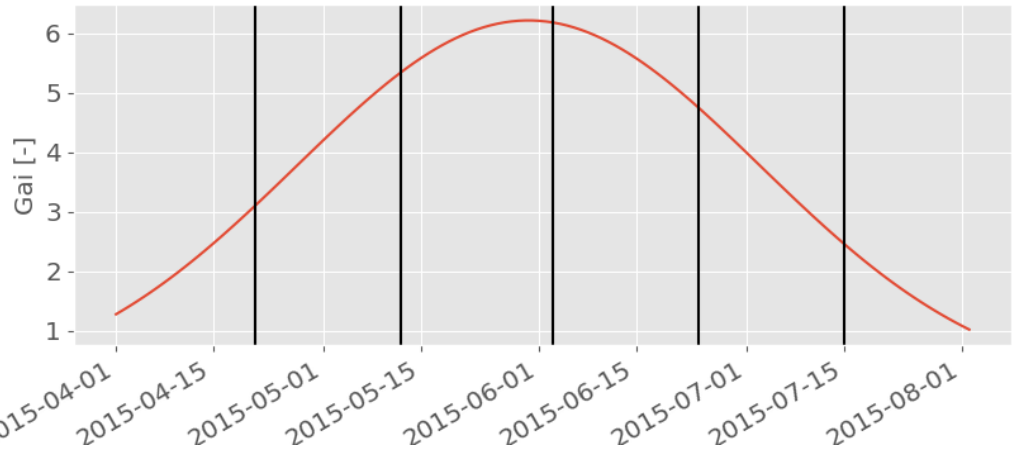

Figure 22 – Time evolution of the GAI along the well-developed vegetation period. The vertical lines are the separation between the distinct sub-periods described in section 2.8.

The periods presented in Figure 22 show that two of them only consider a GAI superior to 4. These periods are the third and the fourth ones. One would expect these periods to have the smallest percentage bias, but it is not the case (Table 13). The percentage bias of the fourth period is indeed the smallest measured, but the one associated with the third period is significantly higher than those related to the first and second period, even if those periods present a GAI between 1 and 5. The assumption trying to link directly the GAI, and the likeliness of the ET and T fluxes does not seem to be met in the framework of this study. One should keep in mind that these conclusions are drawn based on gap-filled transpiration data. It is therefore likely that the relation highlighted by this analysis are slightly biased.

It is also important to note that the T/ET ratio does not only depend on GAI, as showed by the drivers' analysis presented in section 3.8. This ratio would then vary not only with the GAI, but also with the vapour pressure deficit, the net radiation, and the soil water content. It would then be more reasonable to approximate T equal to ET only when no partitioning possibilities are available. This partitioning computation will tend to be more accessible in the future thanks to the development of tools such as Fluxpart or AquaCrop, notably.

4.4 Perspectives

4.4.1 Ecosystem water use efficiency

In the framework of the present discussion, the ecosystem water use efficiency (EWUE) is defined as the ratio of mass of water transpired by the plant and mass of carbon dioxide assimilated via photosynthesis [96]. This parameter is of primary importance for understanding ecosystem functions and water cycle in an evolving agronomical context [96], [97]. Just like in other areas, it has become important to be able to properly estimate the water consumption associated with the growing of a crop [98] with the aim of limiting this water consumption, especially in regions suffering from water scarcity.

Despite the importance and the growing interest in this parameter, problems in its estimation remain. Indeed, the EWUE relating T to GPP, a partitioning of both water vapour and carbon dioxide fluxes has to be conducted [96]. A commonly applied method for partitioning the carbon dioxide flux is to use the procedure developed in [99]. The partitioning of the water vapour flux is usually not computed and the ET is used in the EWUE calculation instead of T [96]. Many uncertainties then remain

from this computation method because of the assumptions usually made [99] and in the consideration of ET instead of T.

However, the Fluxpart model computes water vapour and carbon dioxide fluxes partitioning at the same time with limited assumptions. This model could then allow to better study the EWUE. It would then be interesting to further investigate the possibilities of using Fluxpart to calculate the EWUE.

4.4.2 Model developed by Li and colleagues

There are many other models of ET partitioning into E and T [5], [7], [100] as mentioned in the section 1.2 of the present work. But one model in particular has attracted attention in the course of this work. This latter computes the ET partitioning based on the soil conductance and the vegetation conductance calculation. The conductance separation is computed following the ecosystem conductance model described in a previous study [101], which is a generalization of the Leuning's model [102] and the Medlyn's model [40]. The originality of this approach is that the vegetation conductance is linked to the VPD following a fitted parameter contrary to other conductance models that impose this parameter constant to 0.5 [40] or 1 [102]. In addition to this, contrary to the Fluxpart model, this method doesn't require any prior knowledge about plant WUE [103]. As this model seems to present attractive results and can be implemented at routine eddy-covariance mast [103], it would be interesting to compare its performances with the Fluxpart ones.

5 Conclusion

The partitioning can be done according to many methods and models, but few are commonly used and validated. The aim of this work was therefore to: (i) partition ET into E and T using the FVS and FAO dual-Kc methods, (ii) compare the two methods and estimate their robustness through the characterization of E and T temporal dynamics, and (iii) evaluate the impact of the partitioning on the canopy resistance estimation.

The main results of the present work regarding the first objective are summarized as follow:

- Fluxpart's successful half-hour partitioning is lower than one would expect from the literature. A possible link with the stability parameter is highlighted, but further research is needed.
- The comparison between the E computed with the Beer's law and the one computed via Fluxpart showed good agreement with respect to literature.
- The influence of the intracellular carbon dioxide concentration sub-model choice and the constant-ratio value is greater than expected with a T computed than can go from simple to more than double depending on the sub-model and the value considered.

Considering now the main results relative to the second objective, the following conclusions can be drawn:

- The comparison between the Beer's law' E, the AquaCrop's E and the Fluxpart's E showed that the Fluxpart's E predictions are closer to the Beer's law ones than AquaCrop ones.
- The comparison between the partitioning computed with AquaCrop and the one computed with Fluxpart showed that their general dynamics are similar, but some differences in the magnitudes of the partitioned fluxes were found, with AquaCrop E predictions being superior to Fluxpart's one for the first month on the growing period and AquaCrop predicting an almost null E during the well-developed vegetation period while Fluxpart's one still accounts for a half of the total flux.

Finally, regarding the last objective of this study, the comparison of the canopy resistance when computed with T on the one hand and with ET on the other hand showed significant differences with a convergence between these two simulations when vegetation is well-developed. However, major differences can occur when evaporation rate raises.

In conclusion, Fluxpart's model still need further research, notably regarding the link between the partition success and the stability parameter. Indeed, in the current state of affairs, it would be difficult to consider using this model routinely with an eddy-covariance measurement station because of the too many half-hours for which the partition fails. However, it is important to continue research in this direction, especially by studying a possible application of the model developed by Li and colleagues, given the need to consider T instead of ET in the computation of canopy resistance. It is also interesting to note that the ecosystem water use efficiency could also be computed using the Fluxpart model. This vegetation parameter being at the heart of water management concerns, further research could be carried out on the possibility of using Fluxpart predictions to calculate it.

6 Bibliography

[1] E. Blyth and R. J. Harding, 'Methods to separate observed global evapotranspiration into the interception, transpiration and soil surface evaporation components', *Hydrol. Process.*, vol. 25, no. 26, pp. 4063–4068, Dec. 2011, doi: 10.1002/hyp.8409.

[2] P. Lehmann, O. Merlin, P. Gentine, and D. Or, 'Soil Texture Effects on Surface Resistance to Bare-Soil Evaporation', *Geophys. Res. Lett.*, vol. 45, no. 19, p. 10,398-10,405, Oct. 2018, doi: 10.1029/2018GL078803.

[3] C. Cisneros Vaca, C. van der Tol, and C. P. Ghimire, 'The influence of long-term changes in canopy structure on rainfall interception loss: a case study in Speulderbos, the Netherlands', *Hydrol. Earth Syst. Sci.*, vol. 22, no. 7, pp. 3701–3719, Jul. 2018, doi: 10.5194/hess-22-3701-2018.

[4] H. G. Jones and F. Tardieu, 'Modelling water relations of horticultural crops: a review', *Sci. Hortic.*, vol. 74, no. 1–2, pp. 21–46, Apr. 1998, doi: 10.1016/S0304-4238(98)00081-8.

[5] D. Kool, N. Agam, N. Lazarovitch, J. L. Heitman, T. J. Sauer, and A. Ben-Gal, 'A review of approaches for evapotranspiration partitioning', *Agric. For. Meteorol.*, vol. 184, pp. 56–70, Jan. 2014, doi: 10.1016/j.agrformet.2013.09.003.

[6] R. L. Scott, T. E. Huxman, W. L. Cable, and W. E. Emmerich, 'Partitioning of evapotranspiration and its relation to carbon dioxide exchange in a Chihuahuan Desert shrubland', *Hydrol. Process.*, vol. 20, no. 15, pp. 3227–3243, Oct. 2006, doi: 10.1002/hyp.6329.

[7] P. C. Stoy *et al.*, 'Reviews and syntheses: Turning the challenges of partitioning ecosystem evaporation and transpiration into opportunities', *Biogeosciences*, vol. 16, no. 19, pp. 3747–3775, Oct. 2019, doi: 10.5194/bg-16-3747-2019.

[8] G. E. van Halsema and L. Vincent, 'Efficiency and productivity terms for water management: A matter of contextual relativism versus general absolutism', *Agric. Water Manag.*, vol. 108, pp. 9–15, May 2012, doi: 10.1016/j.agwat.2011.05.016.

[9] B. D. Newman *et al.*, 'Ecohydrology of water-limited environments: A scientific vision', *Water Resour. Res.*, vol. 42, no. 6, Jun. 2006, doi: 10.1029/2005WR004141.

[10] J. L. Holechek, 'Range Livestock Production, Food, and the Future: A Perspective', *Rangelands*, vol. 31, no. 6, pp. 20–25, Dec. 2009, doi: 10.2111/1551-501X-31.6.20.

[11] R. G. Anderson, X. Zhang, and T. H. Skaggs, 'Measurement and Partitioning of Evapotranspiration for Application to Vadose Zone Studies', *Vadose Zone J.*, vol. 16, no. 13, pp. 1–9, Dec. 2017, doi: 10.2136/vzj2017.08.0155.

[12] R. G. Allen, L. S. Pereira, D. Raes, and M. Smith, *Crop evapotranspiration. Guidelines for computing crop water requirements*. Rome: Food and Agriculture Organization of the United Nations, 1998.

[13] Y. Rothfuss, M. Quade, N. Brüggemann, A. Graf, H. Vereecken, and M. Dubbert, 'Reviews and syntheses: Gaining insights into evapotranspiration partitioning with novel isotopic monitoring methods', *Biogeosciences*, vol. 18, no. 12, pp. 3701–3732, Jun. 2021, doi: 10.5194/bg-18-3701-2021.

[14] G. J. Bowen and S. P. Good, 'Incorporating water isoscapes in hydrological and water resource investigations', *WIREs Water*, vol. 2, no. 2, pp. 107–119, Mar. 2015, doi: 10.1002/wat2.1069.

[15] T. J. Griffis, 'Tracing the flow of carbon dioxide and water vapor between the biosphere and atmosphere: A review of optical isotope techniques and their application', *Agric. For. Meteorol.*, vol. 174–175, pp. 85–109, Jun. 2013, doi: 10.1016/j.agrformet.2013.02.009.

[16] H. L. Penman, 'Natural Evaporation from Open Water, Bare Soil and Grass', *R. Soc.*, vol. 193, no. 1032, pp. 120–145, 1948.

[17] J. L. Monteith, 'Evaporation and environment', *Symp. Soc. Exp. Biol.*, vol. 19, pp. 205–234, 1965.

[18] W. J. Shuttleworth and J. S. Wallace, 'Evaporation from sparse crops-an energy combination theory: EVAPORATION FROM SPARSE CROPS', *Q. J. R. Meteorol. Soc.*, vol. 111, no. 469, pp. 839–855, Jul. 1985, doi: 10.1002/qj.49711146910.

[19] R. J. Lascano, 'A General System to Measure and Calculate Daily Crop Water Use', *Agron. J.*, vol. 92, no. 5, pp. 821–832, Sep. 2000, doi: 10.2134/agronj2000.925821x.
[20] C. C. Daamen and L. P. Simmonds, 'Measurement of Evaporation from Bare Soil and its Estimation Using Surface Resistance', *Water Resour. Res.*, vol. 32, no. 5, pp. 1393–1402, May 1996, doi: 10.1029/96WR00268.
[21] V. B. Bufon, R. J. Lascano, C. Bednarz, J. D. Booker, and D. C. Gitz, 'Soil water content on drip irrigated cotton: comparison of measured and simulated values obtained with the Hydrus 2-D model', *Irrig. Sci.*, vol. 30, no. 4, pp. 259–273, Jul. 2012, doi: 10.1007/s00271-011-0279-z.
[22] M. D. Nosetto, E. G. Jobbágy, A. B. Brizuela, and R. B. Jackson, 'The hydrologic consequences of land cover change in central Argentina', *Agric. Ecosyst. Environ.*, vol. 154, pp. 2–11, Jul. 2012, doi: 10.1016/j.agee.2011.01.008.
[23] S. J. Sutanto, J. Wenninger, A. M. J. Coenders-Gerrits, and S. Uhlenbrook, 'Partitioning of evaporation into transpiration, soil evaporation and interception: a comparison between isotope measurements and a HYDRUS-1D model', *Hydrol. Earth Syst. Sci.*, vol. 16, no. 8, pp. 2605–2616, Aug. 2012, doi: 10.5194/hess-16-2605-2012.
[24] J. M. Norman, W. P. Kustas, and K. S. Humes, 'Source approach for estimating soil and vegetation energy fluxes in observations of directional radiometric surface temperature', *Agric. For. Meteorol.*, vol. 77, no. 3–4, pp. 263–293, Dec. 1995, doi: 10.1016/0168-1923(95)02265-Y.
[25] H. G. Jones, 'Use of infrared thermography for monitoring stomatal closure in the field: application to grapevine', *J. Exp. Bot.*, vol. 53, no. 378, pp. 2249–2260, Nov. 2002, doi: 10.1093/jxb/erf083.
[26] E. Haghighi and D. Or, 'Turbulence-induced thermal signatures over evaporating bare soil surfaces', *Geophys. Res. Lett.*, vol. 42, no. 13, pp. 5325–5336, Jul. 2015, doi: 10.1002/2015GL064354.
[27] H. Hoffmann, H. Nieto, R. Jensen, R. Guzinski, P. Zarco-Tejada, and T. Friborg, 'Estimating evaporation with thermal UAV data and two-source energy balance models', *Hydrol. Earth Syst. Sci.*, vol. 20, no. 2, pp. 697–713, Feb. 2016, doi: 10.5194/hess-20-697-2016.
[28] S. Pau, M. Detto, Y. Kim, and C. J. Still, 'Tropical forest temperature thresholds for gross primary productivity', *Ecosphere*, vol. 9, no. 7, Jul. 2018, doi: 10.1002/ecs2.2311.
[29] P. D. Colaizzi *et al.*, 'Two-source energy balance model estimates of evapotranspiration using component and composite surface temperatures', *Adv. Water Resour.*, vol. 50, pp. 134–151, Dec. 2012, doi: 10.1016/j.advwatres.2012.06.004.
[30] M. Meroni *et al.*, 'Remote sensing of solar-induced chlorophyll fluorescence: Review of methods and applications', *Remote Sens. Environ.*, vol. 113, no. 10, pp. 2037–2051, Oct. 2009, doi: 10.1016/j.rse.2009.05.003.
[31] C. Frankenberg *et al.*, 'New global observations of the terrestrial carbon cycle from GOSAT: Patterns of plant fluorescence with gross primary productivity', *Geophys. Res. Lett.*, vol. 38, no. 17, p. n/a-n/a, Sep. 2011, doi: 10.1029/2011GL048738.
[32] P. Köhler, C. Frankenberg, T. S. Magney, L. Guanter, J. Joiner, and J. Landgraf, 'Global Retrievals of Solar-Induced Chlorophyll Fluorescence With TROPOMI: First Results and Intersensor Comparison to OCO-2', *Geophys. Res. Lett.*, vol. 45, no. 19, p. 10,456-10,463, Oct. 2018, doi: 10.1029/2018GL079031.
[33] X. Lu *et al.*, 'Potential of solar-induced chlorophyll fluorescence to estimate transpiration in a temperate forest', *Agric. For. Meteorol.*, vol. 252, pp. 75–87, Apr. 2018, doi: 10.1016/j.agrformet.2018.01.017.
[34] B. Pagán, W. Maes, P. Gentine, B. Martens, and D. Miralles, 'Exploring the Potential of Satellite Solar-Induced Fluorescence to Constrain Global Transpiration Estimates', *Remote Sens.*, vol. 11, no. 4, p. 413, Feb. 2019, doi: 10.3390/rs11040413.
[35] A. J. Rigden and G. D. Salvucci, 'Evapotranspiration based on equilibrated relative humidity (ETRHEQ): Evaluation over the continental U.S.', *Water Resour. Res.*, vol. 51, no. 4, pp. 2951–2973, Apr. 2015, doi: 10.1002/2014WR016072.

[36] A. J. Rigden, G. D. Salvucci, D. Entekhabi, and D. J. Short Gianotti, 'Partitioning Evapotranspiration Over the Continental United States Using Weather Station Data', *Geophys. Res. Lett.*, vol. 45, no. 18, pp. 9605–9613, Sep. 2018, doi: 10.1029/2018GL079121.

[37] P. C. Stoy *et al.*, 'Separating the effects of climate and vegetation on evapotranspiration along a successional chronosequence in the southeastern US', *Glob. Change Biol.*, vol. 12, no. 11, pp. 2115–2135, Nov. 2006, doi: 10.1111/j.1365-2486.2006.01244.x.

[38] L. Misson *et al.*, 'Partitioning forest carbon fluxes with overstory and understory eddy-covariance measurements: A synthesis based on FLUXNET data', *Agric. For. Meteorol.*, vol. 144, no. 1–2, pp. 14–31, May 2007, doi: 10.1016/j.agrformet.2007.01.006.

[39] O. Perez-Priego *et al.*, 'Evaluation of eddy covariance latent heat fluxes with independent lysimeter and sapflow estimates in a Mediterranean savannah ecosystem', *Agric. For. Meteorol.*, vol. 236, pp. 87–99, Apr. 2017, doi: 10.1016/j.agrformet.2017.01.009.

[40] B. E. Medlyn *et al.*, 'Reconciling the optimal and empirical approaches to modelling stomatal conductance', *Glob. Change Biol.*, vol. 17, no. 6, pp. 2134–2144, Jun. 2011, doi: 10.1111/j.1365-2486.2010.02375.x.

[41] M. Berkelhammer *et al.*, 'Convergent approaches to determine an ecosystem's transpiration fraction', *Glob. Biogeochem. Cycles*, vol. 30, no. 6, pp. 933–951, Jun. 2016, doi: 10.1002/2016GB005392.

[42] O. Perez-Priego *et al.*, 'Partitioning Eddy Covariance Water Flux Components Using Physiological and Micrometeorological Approaches', *J. Geophys. Res. Biogeosciences*, vol. 123, no. 10, pp. 3353–3370, Oct. 2018, doi: 10.1029/2018JG004637.

[43] J. A. Nelson *et al.*, 'Coupling Water and Carbon Fluxes to Constrain Estimates of Transpiration: The TEA Algorithm', *J. Geophys. Res. Biogeosciences*, vol. 123, no. 12, pp. 3617–3632, Dec. 2018, doi: 10.1029/2018JG004727.

[44] S. A. Montzka *et al.*, 'On the global distribution, seasonality, and budget of atmospheric carbonyl sulfide (COS) and some similarities to CO_2', *J. Geophys. Res.*, vol. 112, no. D9, p. D09302, May 2007, doi: 10.1029/2006JD007665.

[45] L. Sandoval-Soto and M. Stanimirov, 'Global uptake of carbonyl sulfide (COS) by terrestrial vegetation: Estimates corrected by deposition velocities normalized to the uptake of carbon dioxide (CO2)', p. 8, 2005.

[46] J. E. Campbell *et al.*, 'Photosynthetic Control of Atmospheric Carbonyl Sulfide During the Growing Season', *Science*, vol. 322, no. 5904, pp. 1085–1088, Nov. 2008, doi: 10.1126/science.1164015.

[47] G. Wohlfahrt *et al.*, 'Carbonyl sulfide (COS) as a tracer for canopy photosynthesis, transpiration and stomatal conductance: potential and limitations', *Plant Cell Environ.*, vol. 35, no. 4, pp. 657–667, Apr. 2012, doi: 10.1111/j.1365-3040.2011.02451.x.

[48] K. Gerdel, F. M. Spielmann, A. Hammerle, and G. Wohlfahrt, 'Eddy covariance carbonyl sulfide flux measurements with a quantum cascade laser absorption spectrometer', *Atmospheric Meas. Tech.*, vol. 10, no. 9, pp. 3525–3537, Sep. 2017, doi: 10.5194/amt-10-3525-2017.

[49] M. E. Whelan, T. W. Hilton, J. A. Berry, M. Berkelhammer, A. R. Desai, and J. E. Campbell, 'Carbonyl sulfide exchange in soils for better estimates of ecosystem carbon uptake', *Atmospheric Chem. Phys.*, vol. 16, no. 6, pp. 3711–3726, Mar. 2016, doi: 10.5194/acp-16-3711-2016.

[50] K. Maseyk *et al.*, 'Sources and sinks of carbonyl sulfide in an agricultural field in the Southern Great Plains', *Proc. Natl. Acad. Sci.*, vol. 111, no. 25, pp. 9064–9069, Jun. 2014, doi: 10.1073/pnas.1319132111.

[51] M. E. Whelan *et al.*, 'Reviews and syntheses: Carbonyl sulfide as a multi-scale tracer for carbon and water cycles', *Biogeosciences*, vol. 15, no. 12, pp. 3625–3657, Jun. 2018, doi: 10.5194/bg-15-3625-2018.

[52] T. M. Scanlon and W. P. Kustas, 'Partitioning carbon dioxide and water vapor fluxes using correlation analysis', *Agric. For. Meteorol.*, vol. 150, no. 1, pp. 89–99, Jan. 2010, doi: 10.1016/j.agrformet.2009.09.005.

[53] T. M. Scanlon and P. Sahu, 'On the correlation structure of water vapor and carbon dioxide in the atmospheric surface layer: A basis for flux partitioning', *Water Resour. Res.*, vol. 44, no. 10, Oct. 2008, doi: 10.1029/2008WR006932.
[54] A. S. Monin and A. M. Obukhov, 'Basic laws of turbulent mixing in the surface layer of the atmosphere', *Tr Akad Nauk SSSR Geaphiz Inst*, vol. 24, no. 151, pp. 163–187, 1954.
[55] C. Moureaux, A. Debacq, B. Bodson, B. Heinesch, and M. Aubinet, 'Annual net ecosystem carbon exchange by a sugar beet crop', *Agric. For. Meteorol.*, vol. 139, no. 1–2, pp. 25–39, Sep. 2006, doi: 10.1016/j.agrformet.2006.05.009.
[56] M. Aubinet *et al.*, 'Estimates of the Annual Net Carbon and Water Exchange of Forests: The EUROFLUX Methodology', in *Advances in Ecological Research*, vol. 30, Elsevier, 1999, pp. 113–175. doi: 10.1016/S0065-2504(08)60018-5.
[57] O. Kolle and C. Rebmann, 'EddySoft : documentation of a software package to acquire and process eddy covriance data'. Max-Planck-Institut für Biogeochemie, 2010.
[58] B. Heinesch, 'Lecture on the eddy-covariance method'. 2020.
[59] P. Steduto, *Crop yield response to water*. Rome: Food and Agriculture Organization of the United Nations, 2012.
[60] J. Doorenbos and A. H. Kassam, *Yield response to water*. Rome: Food and Agriculture Organization of the United Nations, 1979.
[61] D. Raes, P. Steduto, T. C. Hsiao, and E. Fereres, 'AquaCrop user manual'. Food and Agriculture Organization of the United Nations, 2012.
[62] P. Paredes, J. P. de Melo-Abreu, I. Alves, and L. S. Pereira, 'Assessing the performance of the FAO AquaCrop model to estimate maize yields and water use under full and deficit irrigation with focus on model parameterization', *Agric. Water Manag.*, vol. 144, pp. 81–97, Oct. 2014, doi: 10.1016/j.agwat.2014.06.002.
[63] H. G. G. C. Nunes *et al.*, 'Parameterization of the AquaCrop model for cowpea and assessing the impact of sowing dates normally used on yield', *Agric. Water Manag.*, vol. 252, p. 106880, Jun. 2021, doi: 10.1016/j.agwat.2021.106880.
[64] B. Heinesch, 'Lecture on the turbulent exchanges'. 2020.
[65] R. J. Hill, 'Implications of the Monin-Obukhov Similarity Theory for Scalar Quantities', Boulder, Colorado, pp. 2236–2244, 1989.
[66] T. H. Skaggs, R. G. Anderson, J. G. Alfieri, T. M. Scanlon, and W. P. Kustas, 'Fluxpart: Open source software for partitioning carbon dioxide and water vapor fluxes', *Agric. For. Meteorol.*, vol. 253–254, pp. 218–224, May 2018, doi: 10.1016/j.agrformet.2018.02.019.
[67] L. Palatella, G. Rana, and D. Vitale, 'Towards a Flux-Partitioning Procedure Based on the Direct Use of High-Frequency Eddy-Covariance Data', *Bound.-Layer Meteorol.*, vol. 153, no. 2, pp. 327–337, Nov. 2014, doi: 10.1007/s10546-014-9947-x.
[68] T. M. Scanlon, D. F. Schmidt, and T. H. Skaggs, 'Correlation-based flux partitioning of water vapor and carbon dioxide fluxes: Method simplification and estimation of canopy water use efficiency', *Agric. For. Meteorol.*, vol. 279, p. 107732, Dec. 2019, doi: 10.1016/j.agrformet.2019.107732.
[69] E. K. Webb, 'On the correction of flux measurements for effects of heat and water vapour transfer', *Bound.-Layer Meteorol.*, vol. 23, no. 2, pp. 251–254, Jun. 1982, doi: 10.1007/BF00123301.
[70] M. Detto and G. G. Katul, 'Simplified expressions for adjusting higher-order turbulent statistics obtained from open path gas analyzers', *Bound.-Layer Meteorol.*, vol. 122, no. 1, pp. 205–216, Jan. 2007, doi: 10.1007/s10546-006-9105-1.
[71] G. G. Katul, S. Palmroth, and R. Oren, 'Leaf stomatal responses to vapour pressure deficit under current and CO_2 -enriched atmosphere explained by the economics of gas exchange', *Plant Cell Environ.*, vol. 32, no. 8, pp. 968–979, Aug. 2009, doi: 10.1111/j.1365-3040.2009.01977.x.
[72] M. T. Sattari, H. Apaydin, and S. Shamshirband, 'Performance Evaluation of Deep Learning-Based Gated Recurrent Units (GRUs) and Tree-Based Models for Estimating ETo by Using

Limited Meteorological Variables', *Mathematics*, vol. 8, no. 6, p. 972, Jun. 2020, doi: 10.3390/math8060972.
[73] D. R. Legates and G. J. McCabe, 'Evaluating the use of "goodness-of-fit" Measures in hydrologic and hydroclimatic model validation', p. 9, 1999.
[74] O. B. Adeboye, B. Schultz, A. P. Adeboye, K. O. Adekalu, and J. A. Osunbitan, 'Application of the AquaCrop model in decision support for optimization of nitrogen fertilizer and water productivity of soybeans', *Inf. Process. Agric.*, p. S2214317320302080, Oct. 2020, doi: 10.1016/j.inpa.2020.10.002.
[75] J. T. Ritchie, 'Model for predicting evaporation from a row crop with incomplete cover', *Water Resour. Res.*, vol. 8, no. 5, pp. 1204–1213, Oct. 1972, doi: 10.1029/WR008i005p01204.
[76] A. Klosterhalfen *et al.*, 'Source partitioning of H2O and CO2 fluxes based on high-frequency eddy covariance data: a comparison between study sites', *Biogeosciences*, vol. 16, no. 6, pp. 1111–1132, Mar. 2019, doi: 10.5194/bg-16-1111-2019.
[77] P. Wagle, P. H. Gowda, B. K. Northup, and J. P. S. Neel, 'Ecosystem-level water use efficiency and evapotranspiration partitioning in conventional till and no-till rainfed canola', *Agric. Water Manag.*, vol. 250, p. 106825, May 2021, doi: 10.1016/j.agwat.2021.106825.
[78] C. Leys, C. Ley, O. Klein, P. Bernard, and L. Licata, 'Detecting outliers: Do not use standard deviation around the mean, use absolute deviation around the median', *J. Exp. Soc. Psychol.*, vol. 49, no. 4, pp. 764–766, Jul. 2013, doi: 10.1016/j.jesp.2013.03.013.
[79] K. T. Zeleke, 'AquaCrop Calibration and Validation for Faba Bean (Vicia faba L.) under Different Agronomic Managements', *Agronomy*, vol. 9, no. 6, p. 320, Jun. 2019, doi: 10.3390/agronomy9060320.
[80] H. Xing *et al.*, 'Global sensitivity analysis of the AquaCrop model for winter wheat under different water treatments based on the extended Fourier amplitude sensitivity test', *J. Integr. Agric.*, vol. 16, no. 11, pp. 2444–2458, Nov. 2017, doi: 10.1016/S2095-3119(16)61626-X.
[81] H. Van Gaelen *et al.*, 'A semi-quantitative approach for modelling crop response to soil fertility: evaluation of the AquaCrop procedure', *J. Agric. Sci.*, vol. 153, no. 7, pp. 1218–1233, Sep. 2015, doi: 10.1017/S0021859614000872.
[82] T. Zhang, J. Su, C. Liu, and W.-H. Chen, 'State and parameter estimation of the AquaCrop model for winter wheat using sensitivity informed particle filter', *Comput. Electron. Agric.*, vol. 180, p. 105909, Jan. 2021, doi: 10.1016/j.compag.2020.105909.
[83] J. Toumi, S. Er-Raki, J. Ezzahar, S. Khabba, L. Jarlan, and A. Chehbouni, 'Performance assessment of AquaCrop model for estimating evapotranspiration, soil water content and grain yield of winter wheat in Tensift Al Haouz (Morocco): Application to irrigation management', *Agric. Water Manag.*, vol. 163, pp. 219–235, Jan. 2016, doi: 10.1016/j.agwat.2015.09.007.
[84] M. Suleau *et al.*, 'Respiration of three Belgian crops: Partitioning of total ecosystem respiration in its heterotrophic, above- and below-ground autotrophic components', *Agric. For. Meteorol.*, vol. 151, no. 5, pp. 633–643, May 2011, doi: 10.1016/j.agrformet.2011.01.012.
[85] D. E. Reed, J. M. Frank, B. E. Ewers, and A. R. Desai, 'Time dependency of eddy covariance site energy balance', *Agric. For. Meteorol.*, vol. 249, pp. 467–478, Feb. 2018, doi: 10.1016/j.agrformet.2017.08.008.
[86] R. Eshonkulov, A. Poyda, J. Ingwersen, A. Pulatov, and T. Streck, 'Improving the energy balance closure over a winter wheat field by accounting for minor storage terms', *Agric. For. Meteorol.*, vol. 264, pp. 283–296, Jan. 2019, doi: 10.1016/j.agrformet.2018.10.012.
[87] K. Wilson *et al.*, 'Energy balance closure at FLUXNET sites', *Agric. For. Meteorol.*, vol. 113, no. 1–4, pp. 223–243, Dec. 2002, doi: 10.1016/S0168-1923(02)00109-0.
[88] H. J. H. Franssen, R. Stöckli, I. Lehner, E. Rotenberg, and S. I. Seneviratne, 'Energy balance closure of eddy-covariance data: A multisite analysis for European FLUXNET stations', *Agric. For. Meteorol.*, vol. 150, no. 12, pp. 1553–1567, Dec. 2010, doi: 10.1016/j.agrformet.2010.08.005.

[89] T. Foken, 'THE ENERGY BALANCE CLOSURE PROBLEM: AN OVERVIEW', *Ecol. Appl.*, vol. 18, no. 6, pp. 1351–1367, Sep. 2008, doi: 10.1890/06-0922.1.
[90] T. M. Scanlon and W. P. Kustas, 'Partitioning Evapotranspiration Using an Eddy Covariance-Based Technique: Improved Assessment of Soil Moisture and Land-Atmosphere Exchange Dynamics', *Vadose Zone J.*, vol. 11, no. 3, p. vzj2012.0025, Aug. 2012, doi: 10.2136/vzj2012.0025.
[91] P. Wagle, T. H. Skaggs, P. H. Gowda, B. K. Northup, and J. P. S. Neel, 'Flux variance similarity-based partitioning of evapotranspiration over a rainfed alfalfa field using high frequency eddy covariance data', *Agric. For. Meteorol.*, vol. 285–286, p. 107907, May 2020, doi: 10.1016/j.agrformet.2020.107907.
[92] J. M. Young-Robertson *et al.*, 'Evaporation dominates evapotranspiration on Alaska's Arctic Coastal Plain', *Arct. Antarct. Alp. Res.*, vol. 50, no. 1, p. e1435931, Jan. 2018, doi: 10.1080/15230430.2018.1435931.
[93] L. Wang-Erlandsson, R. J. van der Ent, L. J. Gordon, and H. H. G. Savenije, 'Contrasting roles of interception and transpiration in the hydrological cycle – Part 1: Temporal characteristics over land', *Earth Syst. Dyn.*, vol. 5, no. 2, pp. 441–469, Dec. 2014, doi: 10.5194/esd-5-441-2014.
[94] G. N. Thorne, I. Pearman, W. Day, and A. D. Todd, 'Estimation of radiation interception by winter wheat from measurements of leaf area', *J. Agric. Sci.*, vol. 110, pp. 101–108, 1987.
[95] L. Horváth, P. Koncz, A. Móring, Z. Nagy, K. Pintér, and T. Weidinger, 'An Attempt to Partition Stomatal and Non-stomatal Ozone Deposition Parts on a Short Grassland', *Bound.-Layer Meteorol.*, Oct. 2017, doi: 10.1007/s10546-017-0310-x.
[96] S. Jiang *et al.*, 'Water use efficiency and its drivers in four typical agroecosystems based on flux tower measurements', *Agric. For. Meteorol.*, vol. 295, p. 108200, Dec. 2020, doi: 10.1016/j.agrformet.2020.108200.
[97] H. Bramley, N. C. Turner, and K. H. M. Siddique, 'Water Use Efficiency', in *Genomics and Breeding for Climate-Resilient Crops*, C. Kole, Ed. Berlin, Heidelberg: Springer Berlin Heidelberg, 2013, pp. 225–268. doi: 10.1007/978-3-642-37048-9_6.
[98] B. Guedes, 'Crop Evapotranspiration and Water Use Efficiency', in *Irrigation Systems and Practices in Challenging Environments*, T. S. Lee, Ed. InTech, 2012. doi: 10.5772/29777.
[99] M. Reichstein *et al.*, 'On the separation of net ecosystem exchange into assimilation and ecosystem respiration: review and improved algorithm', *Glob. Change Biol.*, vol. 11, no. 9, pp. 1424–1439, Sep. 2005, doi: 10.1111/j.1365-2486.2005.001002.x.
[100] J. A. Nelson *et al.*, 'Ecosystem transpiration and evaporation: Insights from three water flux partitioning methods across FLUXNET sites', *Glob. Change Biol.*, vol. 26, no. 12, pp. 6916–6930, Dec. 2020, doi: 10.1111/gcb.15314.
[101] C. Lin, P. Gentine, Y. Huang, K. Guan, H. Kimm, and S. Zhou, 'Diel ecosystem conductance response to vapor pressure deficit is suboptimal and independent of soil moisture', *Agric. For. Meteorol.*, vol. 250–251, pp. 24–34, Mar. 2018, doi: 10.1016/j.agrformet.2017.12.078.
[102] R. Leuning, 'A critical appraisal of a combined stomatal-photosynthesis model for C3 plants', *Plant Cell Environ.*, vol. 18, no. 4, pp. 339–355, Apr. 1995, doi: 10.1111/j.1365-3040.1995.tb00370.x.
[103] X. Li *et al.*, 'A simple and objective method to partition evapotranspiration into transpiration and evaporation at eddy-covariance sites', *Agric. For. Meteorol.*, vol. 265, pp. 171–182, Feb. 2019, doi: 10.1016/j.agrformet.2018.11.017.